catalysts

MDPI

Review

Removal of Organic Dyes from Water and Wastewater Using Magnetic Ferrite-Based Titanium Oxide and Zinc Oxide Nanocomposites: A Review

António B. Mapossa [1,*], Washington Mhike [2], José L. Adalima [3] and Shepherd Tichapondwa [4]

1 Department of Chemical Engineering, Institute of Applied Materials University of Pretoria, Pretoria 0002, South Africa
2 Department of Chemical, Metallurgical and Materials Engineering (Polymer Technology Division), Tshwane University of Technology, Pretoria 0183, South Africa; mhikew@tut.ac.za
3 Department of Archaeology and Anthropology, Eduardo Mondlane University, Maputo 257, Mozambique; jadalima@gmail.com
4 Department of Chemical Engineering, Water Utilization and Environmental Engineering Division, University of Pretoria, Pretoria 0002, South Africa; shepherd.tichapondwa@up.ac.za
* Correspondence: mapossabenjox@gmail.com

Abstract: Heterogeneous photocatalysis using titanium dioxide (TiO_2) and zinc oxide (ZnO) has been widely studied in various applications, including organic pollutant remediation in aqueous systems. The popularity of these materials is based on their high photocatalytic activity, strong photosensitivity, and relatively low cost. However, their commercial application has been limited by their wide bandgaps, inability to absorb visible light, fast electron/hole recombination, and limited recyclability since the nanomaterial is difficult to recover. Researchers have developed several strategies to overcome these limitations. Chief amongst these is the coupling of different semi-conductor materials to produce heterojunction nanocomposite materials, which are both visible-light-active and easily recoverable. This review focuses on the advances made in the development of magnetic ferrite-based titanium oxide and zinc oxide nanocomposites. The physical and magnetic properties of the most widely used ferrite compounds are discussed. The spinel structured material had superior catalytic and magnetic performance when coupled to TiO_2 and ZnO. An assessment of the range of synthesis methods is also presented. A comprehensive review of the photocatalytic degradation of various priority organic pollutants using the ferrite-based nanocomposites revealed that degradation efficiency and magnetic recovery potential are dependent on factors such as the chemical composition of the heterojunction material, synthesis method, irradiation source, and structure of pollutant. It should be noted that very few studies have gone beyond the degradation efficiency studies. Very little information is available on the extent of mineralization and the subsequent formation of intermediate compounds when these composite catalysts are used. Additionally, potential degradation mechanisms have not been adequately reported.

Keywords: magnetic nanoparticles; ferrites; nanocomposites; photocatalytic activity; organic pollutants; reusability

Citation: Mapossa, A.B.; Mhike, W.; Adalima, J.L.; Tichapondwa, S. Removal of Organic Dyes from Water and Wastewater Using Magnetic Ferrite-Based Titanium Oxide and Zinc Oxide Nanocomposites: A Review. *Catalysts* **2021**, *11*, 1543. https://doi.org/10.3390/catal11121543

Academic Editors: Wan Norharyati Wan Salleh, Farhana Aziz and Mohamad Azuwa Mohamed

Received: 12 November 2021
Accepted: 13 December 2021
Published: 18 December 2021

1. Introduction

Nowadays, concern around efficient management of water use has become topical, with interest not only limited to agricultural and industrial sectors but also attracting public health and sustainable economic development proponents.

The wide range of anthropogenic activities that use water results in the generation of highly toxic effluents, which are rich in organic pollutants, rendering them unsuitable for reuse in agricultural activities and human consumption. As a result, water decontamination has become the focus of attention for several studies.

Chemical oxidation-based methods have been proposed as possible remediation techniques for the treatment of domestic and industrial effluents since they are rich in toxic organic compounds, resulting in reduced environmental pollution and enabling the recycling of water resources [1–3].

Advanced oxidative processes (AOPs), which include photocatalysis, plasma oxidation, Fenton's reactions, and ozonation, have been used to degrade numerous pollutants in both water and wastewater treatment applications [2]. Among these, photocatalysis is one of the most widely researched and used AOPs.

Photocatalysis typically involves the irradiation of semi-conductor catalysts with UV or visible light, resulting in the transfer of electrons from the valence band to the conduction band. For charge separation to occur, the energy of the photons must be greater than the band gap energy of the catalyst. The holes (h^+) are capable of reacting with water molecules, leading to the formation of highly reactive hydroxyl radicals (•OH) [3,4].

Titanium dioxide (TiO_2) and zinc oxide (ZnO) are amongst the most widely studied photocatalysts due to their high photocatalytic activity, strong oxidation potential, superhydrophilicity, biological and chemical stability, prolonged durability, non-toxicity, and low cost [4–9].

While these catalysts demonstrate excellent photocatalytic activity, their particle sizes, often in the nano range, negatively impact their recovery. As a result, photocatalysis using these catalysts has limited the large-scale application in treatment of polluted water and wastewater due to the costs associated with loss of the material [4,10,11]. This has necessitated the development of new, inexpensive materials with good photocatalytic efficiency, recoverability, and reusability properties.

Nanomaterials that possess good magnetic properties while exhibiting photocatalytic activity comparable to pure TiO_2 and ZnO are the most ideal photocatalysts as they can be recovered from the reactor using a magnetic field [4].

In particular, ferrite-based nanoparticles have attracted significant attention from researchers in different applications such as sensors, biomedical, catalysis, and energy storage devices. This is due to their excellent adsorption capacities, high surface area, optical properties [12], and magnetic properties [12,13].

The ferrites also present chemical and thermal stability [14,15]. Therefore, nanocomposites of magnetic ferrites-based metal oxides (TiO_2 and ZnO) have been synthesized with the aim of developing photocatalysts with enhanced properties, thereby limiting the deficiencies presented by neat materials.

Several studies show that doping magnetic nanoparticles with ZnO or TiO_2 enhanced the photocatalytic performance of the metal oxides through changes in optical properties, increased surface defects, production of surface oxygen vacancies, and impeding recombination of charge carriers [16,17].

A study conducted by Rahmayeni et al. [18] investigated ferromagnetic $NiFe_2O_4$ doped with diamagnetic ZnO that resulted in superparamagnetic behavior being imparted to the synthesized photocatalyst. They subsequently demonstrated that these properties made it easier to separate the $ZnO/NiFe_2O_4$ nanocomposite from the reaction mixture.

The present work focuses on the development of magnetic spinel ferrite-based zinc oxide and titanium oxide nanocomposites used in the photodegradation of dyes for use in water and wastewater treatment. In particular, principal synthesis and characterization methods are explored.

The recovery and reusability of the magnetic nanocomposite catalysts are reported and discussed. Furthermore, the review also discusses the often overlooked social dimension about the water and wastewater treatment. Finally, conclusions are drawn, and challenges encountered in the use of these catalysts are cited.

2. Magnetic Ferrites Nanoparticles

Ferrites can be divided into four structural groups, which include hexagonal ($MFe_{12}O_{19}$), orthogonal ($MFeO_3$), and garnet ($M_3Fe_5O_{12}$), where *M* represents metal ions, i.e., Ba^{2+} and

$Pb^{2,+}$ and spinel (AB_2O_4) [19]. The cations represented by *A* and *B* occupy tetrahedral and octahedral sites. Figure 1a shows both tetrahedral and octahedral sites coordinated to an oxygen atom [12].

In a single unit cell, there are 64 tetrahedral and 32 octahedral sites where only 8 and 24 sites are occupied by cations, respectively [12]. The distribution of cations in the tetrahedral and octahedral sites of spinel structure can be classified into three groups i.e., normal, inverse, and mixed.

Therefore, normal spinel (Figure 1b) is $ZnFe_2O_4$ where the tetrahedral sites are filled by Zn^{2+}, and the octahedral sites are occupied by Fe^{3+} [12]. Furthermore, the common example for inverse spinel ferrite (Figure 1c) is nickel ferrite, wherein the tetrahedral sites are occupied by half of the Fe^{3+} and octahedral sites are occupied by both Ni^{2+} cations and the other half of Fe^{3+} [20].

$NiFe_2O_4$ demonstrates ferrimagnetic behavior with a curie temperature (T_C) of approximately 858 K, whereas $ZnFe_2O_4$ displays antiferromagnetic behavior ordering below the curie temperature of 9 K [21].

An example of a mixed spinel ferrite is $MnFe_2O_4$, its structure is represented as follows: ($[Mn_{0.8}Fe_{0.2}][Mn_{0.2}Fe_{1.2}]O_4$), where the +2 and +3 ions are distributed randomly on both sites [22]. $CoFe_2O_4$ can be found as an inverse or normal spinel structure; this is dependent on the synthesis method used.

Ferrites have attracted more attention in catalysis for water and wastewater treatment due to their various advantages such as the presence of a band gap capable of absorbing visible light, together with the spinel crystal structure, which increases photocatalytic activity due to the catalytic sites t featured on the crystal lattice [23].

Besides the magnetic behavior, other properties that spinel ferrites possess include spin canting effect, spin-glasslike behavior, and higher heat and corrosion resistance [12,22]. The common band gap energies for some spinel ferrites are as follows: $CuFe_2O_4$ (1.32 eV), $ZnFe_2O_4$ (1.92 eV), $CoFe_2O_4$ (2.27 eV), and $NiFe_2O_4$ (2.19 eV) [23,24].

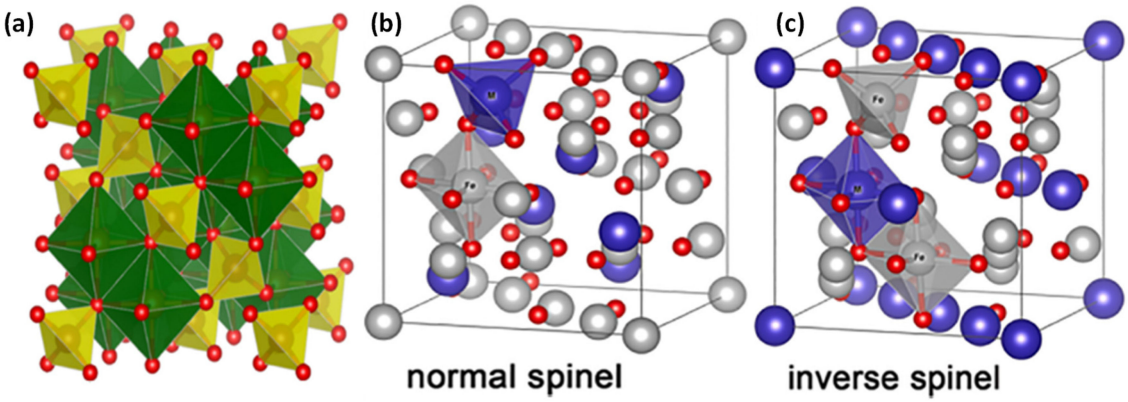

Figure 1. Structure of magnetic spinel ferrite showing tetrahedral sites (yellow), octahedral sites (green), and oxygen atoms (red) units (**a**) [12]. Unit cell structure of (**b**) normal spinel ferrite, and (**c**) inverse spinel ferrite [25]. Republished with permission from Elsevier.

Due to the small band gap energy of ferrites, which makes them effective under absorption of visible light irradiation, they are extremely suitable for the removal of organic pollutants in water and wastewater treatment processes [22,23].

2.1. Methods of Synthesis of Magnetic Spinel Ferrites

Synthesis methods play an important role in the development of magnetic nanoparticles as this controls the electrical, optical, and magnetic properties of the material [15].

Additionally, synthesis methods should pay particular attention to the cost of production. An optimum balance between processing costs and the desired nanomaterial properties is desired [15,26].

Numerous synthesis methods have been used to prepare magnetic nanoparticles (MNPs); these include microwave [27–29], sonochemical [30], sol-gel [31–34], co-precipitation [35,36], combustion [37,38], micro-emulsion [39], and hydrothermal [40–44]. Amongst these, co-precipitation, sol-gel, hydrothermal, and combustion methods are the most widely reported.

Co-precipitation requires careful monitoring of pH in order to obtain pure spinel ferrites [25]. Advantages associated with this method include low cost, short synthesis time, high product yield, and production of uniformly sized particles [45].

For example, El-Okr et al. [46] synthesized magnetic $CoFe_2O_4$ using the co-precipitation method and obtained crystallites between 11 and 45 nm in size, with saturation magnetization ranging from 5 to 67 emu/g. The authors reported that the difference in crystallite size and saturation magnetization (*Ms*) values was associated with the variation of parameters such as pH and calcination temperature.

The hydrothermal synthesis method enables particle size control and flexibility in terms of surface modification. It is based on the wet-chemical synthesis; typically, this occurs in sealed reactors or autoclaves at high vapor pressures (from 0.3 to 4 MPa) and elevated temperatures (130 to 250 °C) [47,48].

Some noteworthy advantages of this method include low temperature for synthesis, high purity, simple reactions, cost-effectiveness, and good dispersibility of the MNPs [49]. For instance, Zhao et al. [41] prepared cobalt ferrite using the hydrothermal method. The resultant material had 70 nm crystallites with a saturation magnetization (Ms) of 86 emu/g.

The sol-gel method is extensively used for the synthesis of spinel ferrites [50–55]. The process involves the transition of a system from a liquid phase (sol) to a solid phase (gel), through chemical reactions such as hydrolysis and condensation polymerization of the metallic precursors [25]. Thus, its widespread acceptance is driven by the low cost associated with the method, better homogeneity, composition control, and narrow particle size distribution at relatively low temperatures [25,45].

The sol–gel method also allows for good control of the structural and magnetic properties of MNPs [45]. Sajjia et al. [56] prepared cobalt ferrite nanoparticles by a sol-gel method. Their results demonstrated that the saturation magnetization was 67.3 emu/g and the particle sizes were between 7 and 28 nm, according to the calcination temperature of nanoparticles.

The combustion synthesis method of MNPs is based on the thermodynamics principles and chemistry of propellants and explosives [57–59]. The method requires a powdered mixture, typically consisting of an oxidizing agent containing the metal ions of interest such as oxidizing reagents, and a reducing agent such as urea or glycine [57,60–63].

Upon ignition, the mixture undergoes an exothermic or endothermic redox reaction depending on the material properties. Equation (1) shows the combustion reaction used to produce $ZnFe_2O_4$ by Mapossa et al. [64].

$$Zn(NO_3)_2{\cdot}6H_2O_{(s)} + 2Fe(NO_3)_3{\cdot}9H_2O_{(s)} + 6.67(NH_2)_2CO_{(s)} \rightarrow ZnFe_2O_{4(s)} + 6.67CO_{2(g)} + 37.33H_2O_{(g)} + 10.67N_{2(g)} \quad (1)$$

Using the principles of propellant chemistry, the valences of the elements present in the oxidizing and reducing agents are represented as follows: Zn = +2; Fe = +3; C = +4; H = +1; and O = −2. The total valence of urea is equal to +6, and the total valence of nitrates ($Zn(NO_3)_2/Fe(NO_3)_3$, 1/2) for oxidizing agent zinc ferrite ($ZnFe_2O_4$) is equal to −40.

Thus, the combination of total valences of reducing agent (fuel, urea) and oxidizing agent achieved gives the following expression: $-40 + 6n = 0$, where n is the number of moles of urea (in this case, n = 6.67 mol) for the combustion reaction. Since it is complete combustion, the stoichiometric reaction ($\Phi e = 1$) follows the definition described for the oxygen balance and equals zero.

To accomplish this, the content of oxygen from the nitrates is completely oxidized by a reducing agent (fuel) in the mixture [61].

A study conducted by Salunkhe et al. [65] evaluated the magnetic properties of cobalt ferrite nanoparticles prepared using the combustion method using glycine as fuel. The results showed that the crystallite size was 38 nm and saturation magnetization was

67.3 emu/g. Table 1 summarizes the structural and magnetic properties of $CoFe_2O_4$ MNPs synthesized using various methods.

Table 1. Effect of synthesis method in structural and magnetic properties of catalyst cobalt ferrite [65–67].

Synthesis Method	Sol-Gel	Co-Precipitation	Hydrothermal	Combustion
Crystallite size (nm)	37.3	33.0	15.0	38.0
Ms (emu·g^{-1})	58.9	60.9	56.9	59.0

2.2. Characterization Methods

Before the synthesized magnetic materials are used as catalysts, an investigation of the various properties, which influence their performance, is essential. Some of the key parameters are size, shape, and surface area.

Therefore, this information can be elucidated using one or a combination of the following techniques: X-ray diffraction (XRD), scanning electron microscopy (SEM), transmission electron microscopy (TEM), BET-N_2 analysis, vibrating sample magnetometer (VSM).

X-ray diffraction (XRD) gives information about the structural properties, crystallite size, and crystalline phases of magnetic nanoparticles as catalysts.

The BET-N_2 adsorption-desorption isotherm is a technique commonly used to evaluate the porosity and specific surface area of MNPs. For example, smaller particles have a larger surface area, leading to higher photocatalytic activity due to a larger number of active sites [23]. More details are explained in Section 5.

The magnetic behavior of the ferrites (saturation magnetization) is evaluated using a vibrating sample magnetometer (VSM). The information obtained from this technique gives an idea of the recovery potential of the photocatalyst.

Figure 2 shows the magnetic behavior of various ferrites at room temperature. With the exception of zinc ferrite, which has a low magnetization of saturation, the other ferrites have a high magnetization of saturation values, which implies good magnetic and recyclability properties [67].

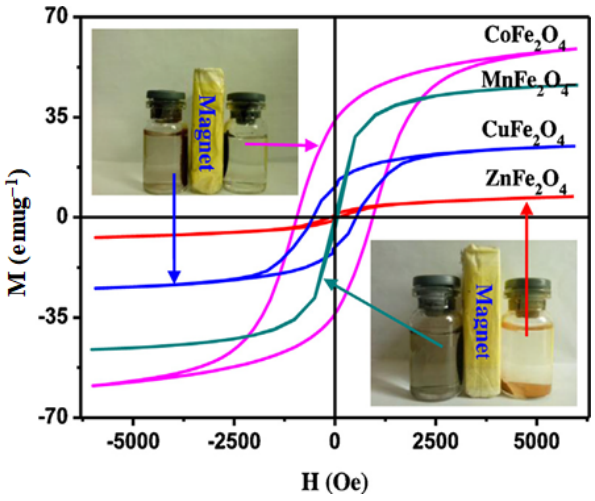

Figure 2. Magnetic properties behavior of different photocatalysts at room temperature [67]. Republished with permission from Elsevier.

The morphology, including shape, and particle size of magnetic nanoparticles, can be determined using transmission electron microscopy (TEM) and scanning electron microscopy (SEM). Figure 3a,b demonstrates the difference in morphology and structure of cobalt ferrite affected by different methods of synthesis [68].

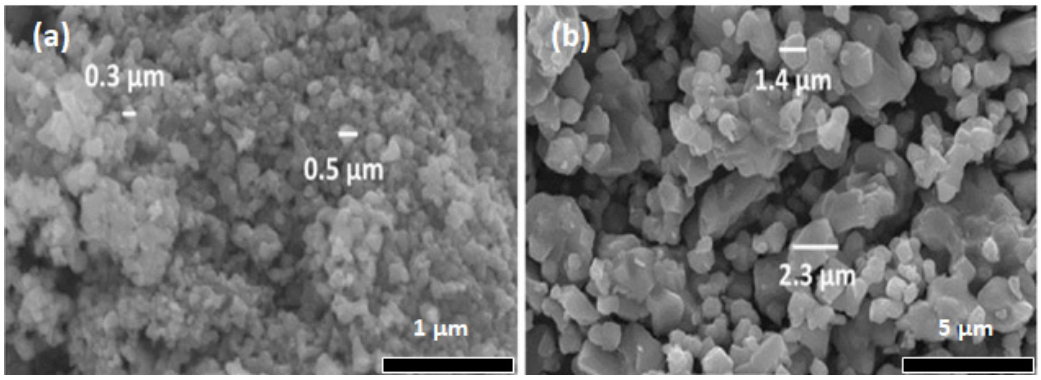

Figure 3. SEM micrographs for $CuFe_2O_4$ obtained by different methods: (**a**) Sol-Gel method and (**b**) hydrothermal synthesis. The images show the effect of methods of synthesis for the materials obtained [68]. Republished with permission from Elsevier.

Thermal decomposition studies are crucial for the development of nanocatalysts as most of them are synthesized at high temperatures. Thermogravimetric analysis (TGA) or differential scanning calorimetry (DSC) are used to determine the optimum temperature required for the synthesis of magnetic nanoparticles due to the possibility of a loss of activity during their preparation.

Finally, these characterization techniques are also employed to investigate if any changes occur by decomposition or degradation, and whether they retain their magnetic properties after the photocatalytic process.

3. Photocatalytic Application of Magnetic Ferrites and Their Nanocomposites

Photocatalytic degradation is a sequence of chemical reactions promoted by light resulting in the breakdown of the target compound [69].

The photocatalytic activity is effectively dependent on the surface area and electron-holes separation efficiency of the catalyst [69]. Figure 4 shows a schematic of the photocatalytic mechanism of magnetic $ZnFe_2O_4/ZnO$ nanocomposite during methylene blue and methylene orange dye degradation [69].

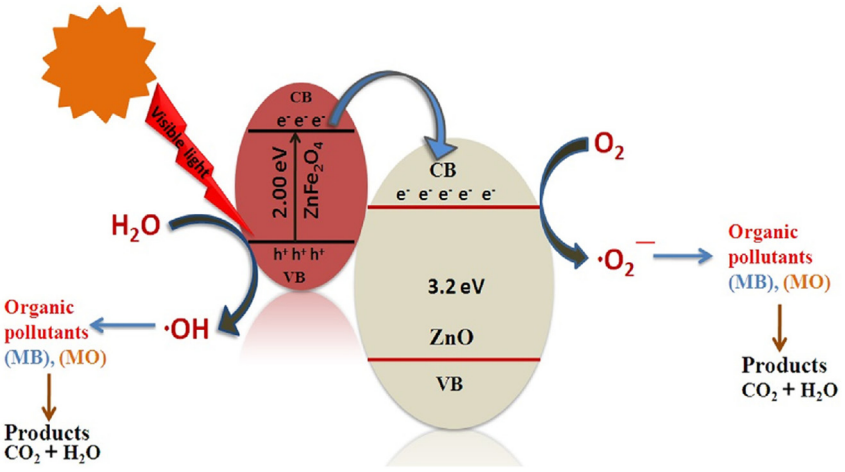

Figure 4. A general scheme of visible light photodegradation mechanism of magnetic nanocomposite i.e., $ZnFe_2O_4/ZnO$ for organic pollutants [69]. Republished with permission from Elsevier.

It has been reported that nanocatalysts that have high surface areas exhibit higher photocatalytic activity compared to their larger counterparts with lower surface area. The smaller nanoparticles support the easy transition of electrons from the valence to conduction band, thereby generating electron-hole pairs when exposed to UV-visible radiation.

The generated electrons and holes further interact with dissolved oxygen and water to produce highly reactive free radical species capable of degrading the methylene dyes [69,70]. The general photocatalytic degradation mechanism of magnetic nanocomposites towards organic pollutants is demonstrated by Equations (2)–(8).

$$ZnO + h\nu \rightarrow h^+ + e^- \quad (2)$$

$$ZnFe_2O_4/ZnO \rightarrow ZnFe_2O_4/ZnO\ (e^-) \quad (3)$$

$$e^- + O_{2\ absorbed} \rightarrow \bullet O_2{}^- \quad (4)$$

$$\bullet O_2{}^- + \text{MB dye} \rightarrow \text{degraded products} \quad (5)$$

$$h^+ + H_2O_{absorbed} \rightarrow H^+ + \bullet OH \quad (6)$$

$$h^+ + OH_{absorbed}{}^- \rightarrow \bullet OH \quad (7)$$

$$\bullet OH + \text{MB dye} \rightarrow \text{degraded products} \quad (8)$$

Reduction and oxidation take place at the photo-excited surface of the photocatalyst. Recombination between e^- and h^+ can occur for the use of redox reaction. The e^- and h^+ that do not recombine are transferred to the surface of redox reaction and undergo reduction process and oxidation process to form superoxide ion ($O_2{}^-$) and ·OH, respectively. OH^- then leads to the production of strong oxidizing ·OH radicals. Meanwhile, the negative e^- reacts with the oxygen (O) molecule to form a $\cdot O_2{}^-$. This $\cdot O_2{}^-$ also produces ·OH radicals via the formation of $HO_2{}^\bullet$ radicals and H_2O_2. The radicals formed from the reaction are used to degrade the organic pollutant [71,72].

3.1. Nickel Ferrite and Nanocomposites

$NiFe_2O_4$ has generated a lot of interest because of its excellent features. These include being a soft ferrimagnetic or ferrite *n*-type semiconductor with low coercivity, chemical stability, and electrical resistivity. These make it an excellent material in different applications such as in magnetic resonance imaging enhancement, magnetic recording media, and electronic devices, as well as in catalysis [20].

Following the description in Section 2, $NiFe_2O_4$ is completely composed of an inverse spinel structure comprising a face-centered cubic lattice. $NiFe_2O_4$ consists of tetrahedral sites occupied by half of the Fe^{3+} cations, while the rest of the Fe^{3+} and Ni^{2+} cations are distributed over the octahedral sites [73–75].

Figure 5 shows the XRD spectra and SEM images of neat zinc oxide, nickel ferrite, and their nanocomposites [76]. In the study conducted by Adeleke et al. [76], no secondary peaks or secondary phases of material were observed; this demonstrated the effectiveness of the synthesis method used in this study.

Furthermore, SEM images demonstrated the effect of doping ferrite with zinc oxide. The high degree of agglomeration and different morphologies observed on the ZnO/Fe_2O_4 catalyst were attributed to the magnetic attraction between nickel ferrite and zinc oxide layers [76].

Several studies have demonstrated that magnetic $NiFe_2O_4$ and its nanocomposites are effective photocatalysts for the removal of dye from water and wastewater, due to their high adsorption capacity and strong photocatalytic properties [16,77–82].

Khosravi and Eftekhar [83] synthesized magnetic $NiFe_2O_4$ using a sol-gel method and evaluated its effectiveness as an adsorbent for the removal of Reactive Blue 5 (RB5) dye. Parameters such as pH, temperatures, and catalyst concentration were evaluated during RB5 degradation [83]. Maximum degradation (90%) was achieved under acidic conditions (pH = 1) at room temperature using an (adsorbent/catalyst loading of 0.03 g/L).

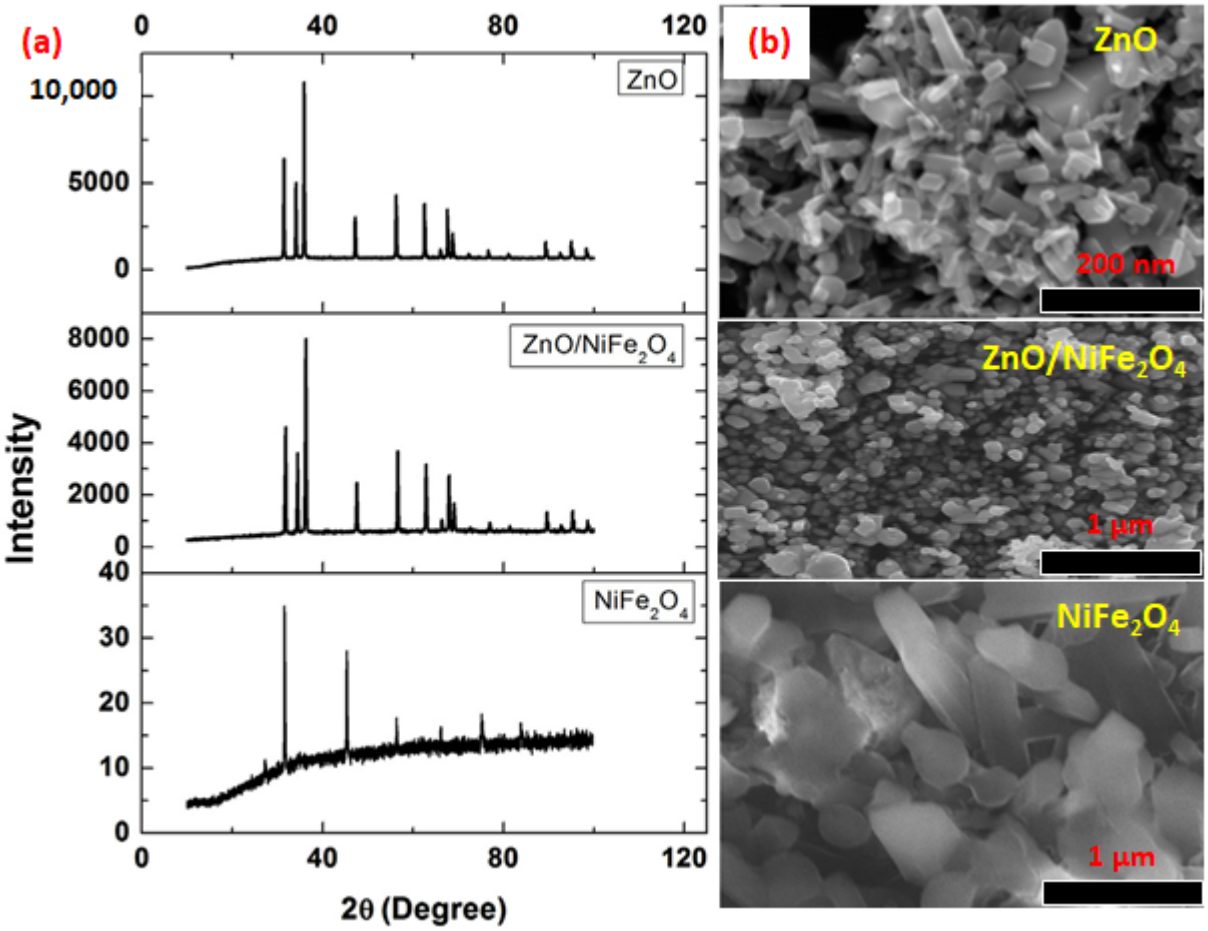

Figure 5. (**a**) XRD structural and (**b**) SEM micrographs of ZnO, $NiFe_2O_4$, and magnetic $ZnO/NiFe_2O_4$ nanocomposites [76]. Republished with permission from Elsevier.

These findings were corroborated by Zhu et al. [16] when they evaluated the photocatalytic degradation of Congo Red dye using $NiFe_2O_4/ZnO$ as a catalyst. In their study, the $NiFe_2O_4/ZnO$ nanocomposite resulted in a 94% removal of Congo red solution under simulated solar light irradiation in 10 min. Nickel ferrite was also shown to be effective when coupled with other metal oxides such as TiO_2.

In a study done by Hung and Thanh [84], a magnetic nanocomposite of $NiFe_2O_4/TiO_2$ degraded 98% of methyl orange dye after 14 h of UV or visible light irradiation. Although the reaction time was rather long, the photocatalyst had a high saturation of magnetization (40 emu/g), which makes it easily recyclable for reuse.

The results obtained in these studies demonstrate that nickel ferrite nanocomposites are potential candidates for wastewater treatment in large-scale applications.

Additional studies that illustrate the efficacy of nickel ferrite, nickel ferrite-based titanium oxide, and zinc oxide catalysts in the degradation of variant organic pollutants are summarized in Table 2.

3.2. Zinc Ferrite and Nanocomposites

Zin ferrite has a small bandgap of around 1.9 eV, which gives a good response to the visible light, as well as excellent photochemical stability, considerable magnetism, and cost-effectiveness. As a result, it has also attracted attention by researchers in the photocatalysis process [85].

The compound consists of a fully normal spinel structure, where its tetrahedral sites are occupied only by Zn^{2+} cations and the Fe^{3+} ions are distributed in the octahedral

sites [86]. Figure 6 shows the XRD patterns and SEM micrographs of the zinc oxide-, zinc ferrite-, and zinc ferrite-based zinc oxide nanocomposites [17].

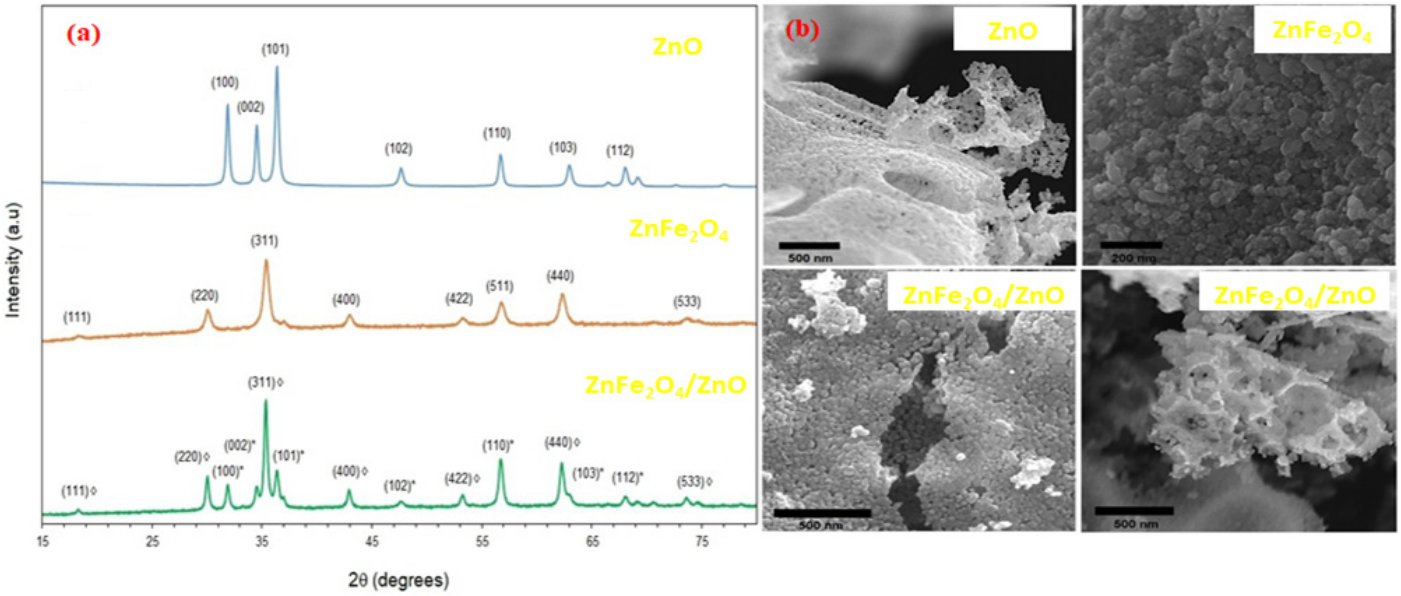

Figure 6. (**a**) XRD structural and (**b**) SEM micrographs of ZnO, $ZnFe_2O_4$, and magnetic $ZnFe_2O_4$/ZnO nanocomposites with different molar ratios (1/1, 1/8) [17]. ◊ corresponds to $ZnFe_2O_4$ and * corresponds to ZnO. Republished with permission from Wiley.

The photocatalyst $ZnFe_2O_4$/ZnO had diffraction peaks similar to those of neat $ZnFe_2O_4$ and ZnO. The sharp peaks showed good crystallinity of the nanocomposite [17], which demonstrates the efficacy of the synthesis method used in this study.

The SEM images revealed the effect of incorporating $ZnFe_2O_4$ nanoparticles into the pores of the ZnO matrix. The authors observed that a high content of ZnO nanoparticles was formed; these were better defined in the $ZnFe_2O_4$/ZnO nanocomposites [17].

Significant efforts have been devoted to investigating $ZnFe_2O_4$-based photocatalysts for water and wastewater treatment, with the aim of removing organic pollutants [87–90].

Yuan et al. [91] investigated the photocatalytic activity of a $ZnFe_2O_4/TiO_2$ nanocomposite where the pure $ZnFe_2O_4$ and TiO_2 were obtained via the co-precipitation method. The results showed that the $ZnFe_2O_4/TiO_2$ and pure TiO_2 resulted in 95% and 20% of degradation of phenol respectively during 180 min of irradiation under UV–Visible. This demonstrated that the $ZnFe_2O_4/TiO_2$ nanocomposite catalyst was more effective than pure TiO_2 in the degradation of phenol.

In addition, Shao et al. [85] evaluated the application of $ZnFe_2O_4$/ZnO nanoparticles in the photodegradation of methylene blue dye. The findings demonstrated that even after three cycles, the photocatalytic activity of the magnetic nanocomposite $ZnFe_2O_4$/ZnO (65%) was better compared to that of pure ZnO (58%), indicating the significance of $ZnFe_2O_4$ in the suppression of ZnO photo-corrosion. This was attributed to the photostability of $ZnFe_2O_4$ nanoparticles [92].

Further study by Patil et al. [93] investigated the photocatalytic activity of $ZnFe_2O_4$ nanoparticles synthesized using a combustion method. Their activity was tested on synthetic wastewater made up of the following dyes: Methylene Blue, Rose Bengal, Evans Blue, and Indigo Carmine.

Degradation efficiencies of 98, 99, 82, and 87% were recorded for each dye, respectively [93]. The antibacterial activity of $ZnFe_2O_4$ against diverse gram-negative bacterial strains such as *Staphylococcus aureus*, *Pseudomonas aeruginosa*, *Escherichia coli*, and *Bacillus* was also investigated. A variation in the antibacterial activity towards the different bacterial strains was observed [93].

Other work conducted by Sripriya et al. [94] reported on the excellent photocatalytic performance of $ZnFe_2O_4$ in the degradation of 4-chlorophenol (4-CP). They further reported that factors such as particle size and surface area significantly affected the activity. Further studies on the use of magnetic ZnF_2O_4 nanocomposites as photocatalysts are listed in Table 2.

3.3. Cobalt Ferrite and Nanocomposites

Cobalt ferrite is a hard ferrimagnetic material that has a face centered cubic structure [95]. It exists as a normal spinel structure or inverse spinel structure, depending on the synthesis method. In the normal spinel structure, the Co^{2+} ions are distributed in the tetrahedral sites, while the octahedral sites are occupied by Fe^{3+} ions.

For the inverse spinel structure, the tetrahedral sites are occupied by half of the Fe^{3+} ions and the rest of the octahedral sites are distributed by Fe^{3+} and Co^{2+} ions. It is important to note that the magnetic properties vary depending on the structures [95,96].

Figure 7 shows the XRD patterns and TEM micrographs of the cobalt ferrite and cobalt ferrite-based zinc oxide nanocomposite [97]. Pristine XRD patterns were obtained with no impurities; this demonstrated that the co-precipitation method used for synthesis was highly efficient [97].

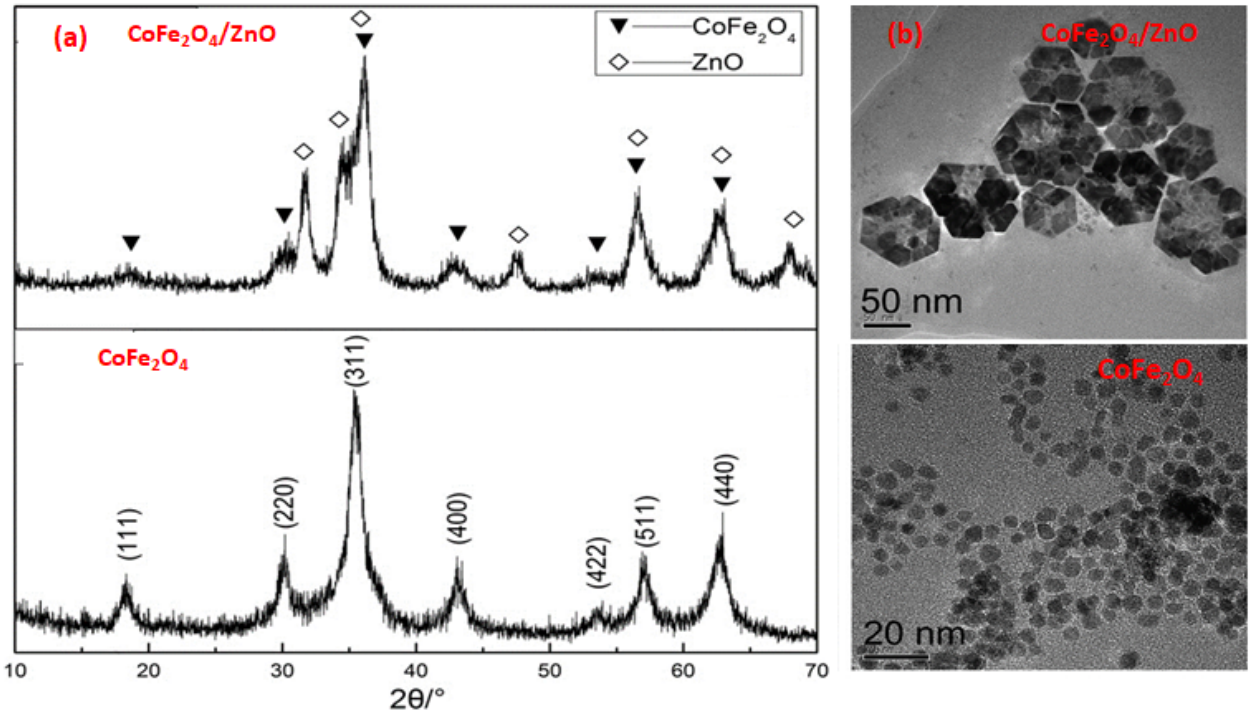

Figure 7. (**a**) XRD structural and (**b**) TEM micrographs of $CoFe_2O_4$ and magnetic $CoFe_2O_4$/ZnO nanocomposites [97]. Republished with permission from Elsevier.

Several studies have demonstrated the potential of cobalt spinel ferrite doped with metals oxides (TiO_2 or ZnO) as photocatalysts for water and wastewater treatment for organic pollutants removal. This is due to the various attributes that include chemical stability, small band-gap energy that leads to activation by visible light [5,12,98–100], magnetic properties, and higher surface area.

A study conducted by de Oliveira et al. [4] demonstrated that the magnetic nanocatalyst of $CoFe_2O_4$ coupled to TiO_2 resulted in 100% degradation of diuron degradation. This study also observed that $CoFe_2O_4/TiO_2$ nanoparticles displayed good saturation magnetization, demonstrating that they can be easily separated for reuse.

Furthermore, Li et al. [101] reported good performance of magnetic $TiO_2/CoFe_2O_4$ nanocomposite for methylene blue (MB) degradation (98%) in 300 min. The good per-

formance of magnetic $TiO_2/CoFe_2O_4$ nanocomposite was attributed to the presence of $CoFe_2O_4$, which not only improved the UV light absorbance but also enhanced the response to the visible light region.

A study done by Chandel et al. [102] reported that the $ZnO/CoFe_2O_4$ nanocomposite displayed 94% degradation efficiency towards Methylene Orange (MO) and 92% removal for malachite green (MG) dye. The authors attributed the hydroxyl radicals ($OH^{\bullet}$) and holes (h^+_{VB}) as the main reactive species responsible for the degradation of MO and MG dyes.

The photocatalytic activity and stability of $ZnO/CoFe_2O_4$ were confirmed by showing 10 cycles for successive reuse. Since $ZnO/CoFe_2O_4$ is recyclable and easily recovered magnetically; it is a good candidate for use as a low-cost photocatalyst for water and wastewater treatment.

Additional studies on the photocatalytic performance of cobalt ferrite and their nanocomposites in the degradation of organic pollutants are summarized in Table 2.

3.4. Manganese Ferrite and Nanocomposites

$MnFe_2O_4$ is a soft spinel ferrite with high magnetic permeability and moderate saturation magnetization, high chemical stability, high electrical resistance, and special optical properties [103]. A combination of these factors makes it attractive for use in different applications such as biomedical drug delivery and catalysis [103,104].

$MnFe_2O_4$ is considered a mixed spinel ferrite in which the tetrahedral and octahedral sites are both are occupied by Mn^{2+} and Fe^{3+} ions [104,105]. High reaction temperatures affect the synthesis of the magnetic ferrite, resulting in variation in particle sizes of the material, which in turn affects other parameters such as saturation magnetization.

A study conducted by Chang et al. [106] demonstrated through X-ray diffraction analysis that no other peaks attributed a second phase were observed for manganese ferrite and titanium oxide. Additionally, peaks attributed to pure materials ($MnFe_2O_4$ and TiO_2) were observed in the XRD pattern of $MnFe_2O_4/TiO_2$ nanocomposite (Figure 8).

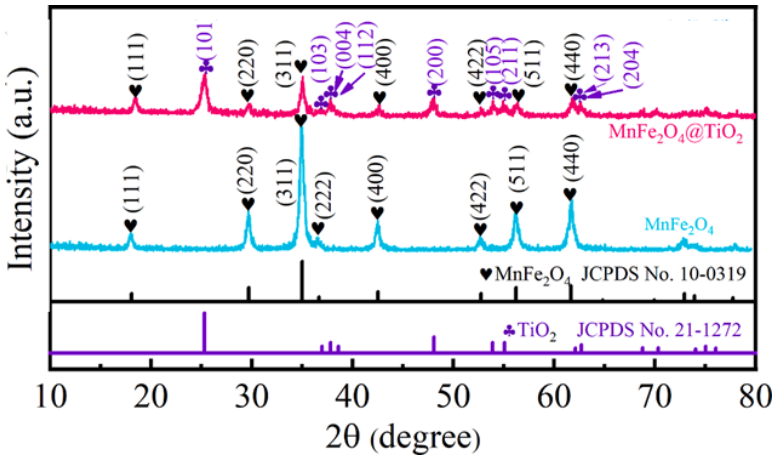

Figure 8. XRD patten of $MnFe_2O_4$ and $MnFe_2O_4/TiO_2$ nanocomposites [106]. Republished with permission from Elsevier.

The findings demonstrate that the magnetic nanoparticles were successfully synthesized via a hydrothermal followed by the sol-gel method [106]. The SEM micrograph of $MnFe_2O_4/TiO_2$ (Figure 9) showed that agglomerated spherical particles were produced.

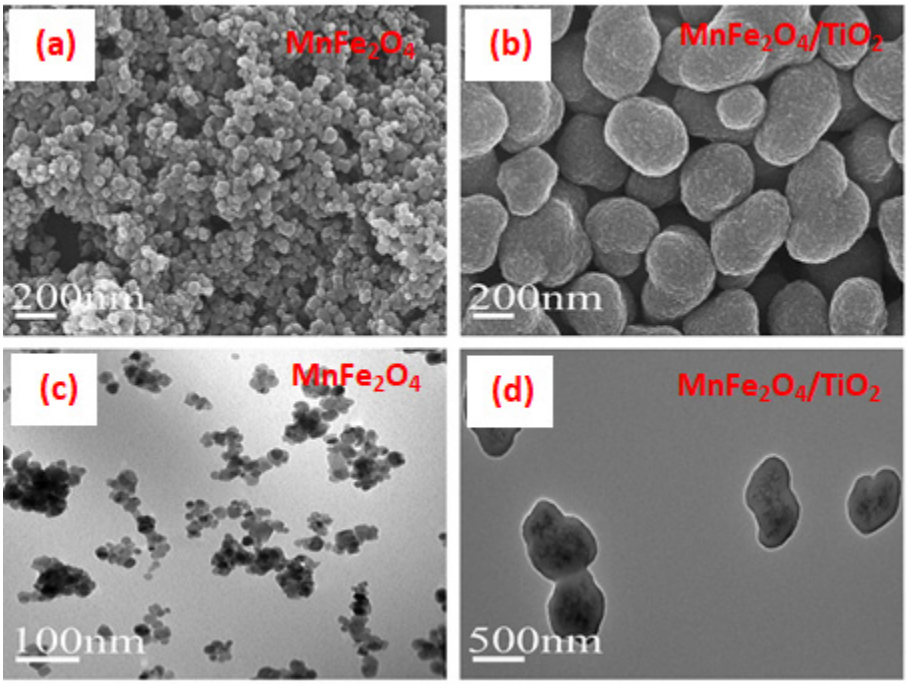

Figure 9. SEM micrographs of: (**a**) $MnFe_2O_4$; (**b**) $MnFe_2O_4/TiO_2$ nanocomposite; and TEM images of (**c**) $MnFe_2O_4$ and (**d**) $MnFe_2O_4/TiO_2$ nanocomposites [106]. Republished with permission from Elsevier.

The $MnFe_2O_4$ nanoparticles display a well-defined morphology with particle size around 15–20 nm. Meanwhile, it is clearly visible that the particle size of $MnFe_2O_4/TiO_2$ is uneven and relatively large [106].

The TEM micrographs of photocatalyst $MnFe_2O_4/TiO_2$ demonstrated that $MnFe_2O_4$ nanoparticles are coated by TiO_2 with shape a core-shell structure (see Figure 9) [106].

Numerous studies have demonstrated that manganese ferrite-based metal oxide nanocomposites are effective in the photocatalytic degradation of organic dyes. For example, Zamani et al. [107] evaluated the photocatalytic performance of a magnetic $MnFe_2O_4/ZnO$ nanocomposite for Congo red dye (CR) removal.

The results showed that 90% degradation of Congo red dye was achieved in 35 min under UV-vis irradiation. Additionally, Arief et al. [103] showed that the same nanocomposite was effective for Rhodamine B dye degradation (95%). This was attributed to the presence of a narrow band gap energy (1.95 eV) of $MnFe_2O_4/ZnO$.

Silambarasu et al. [108] tested the performance of $MnFe_2O_4$ on the degradation of methylene blue dye. The manganese ferrite achieved 96% dye decolorization and exhibited saturation magnetization (*Ms*) of 39.7 emu/g. The magnetic properties indicated that the product could be easily recovered for potential reuse.

There are few studies reporting the application of manganese ferrite and manganese ferrite-based zinc oxide and titanium oxide nanocomposites in water and wastewater treatment for organic pollutants removal.

3.5. Copper Ferrite and Nanocomposites

$CuFe_2O_4$ is one of the magnetic nanoparticles that has become a promising candidate in the catalysis field due to the presence of surface hydroxyl groups, good chemical, and thermal stabilities, a small band gap, and magnetic properties [109]. These characteristics make it attractive as a photocatalyst for work on water and wastewater treatment for organic pollutants degradation.

Copper ferrite has an inverse spinel structure, where the tetrahedral sites are occupied by half of the Fe^{3+} ions and the rest of the octahedral sites are occupied by Fe^{3+} and Cu^{2+} ions [110]. Therefore, besides the cubic crystal structure, the copper ferrite also

presents a tetragonal crystal structure that depends on the synthesis method and annealing temperature [110].

In the XRD patterns of $TiO_2/CuFe_2O_4$ nanocomposites, the peaks associated with the neat TiO_2 and $CuFe_2O_4$ were observed without any further secondary phase (Figure 10) [109]. This demonstrated that the nanocomposite photocatalyst was successfully prepared using the Sol-Gel method and the pure titanium oxide and copper ferrite nanoparticles remained with their structure during the synthesis processes.

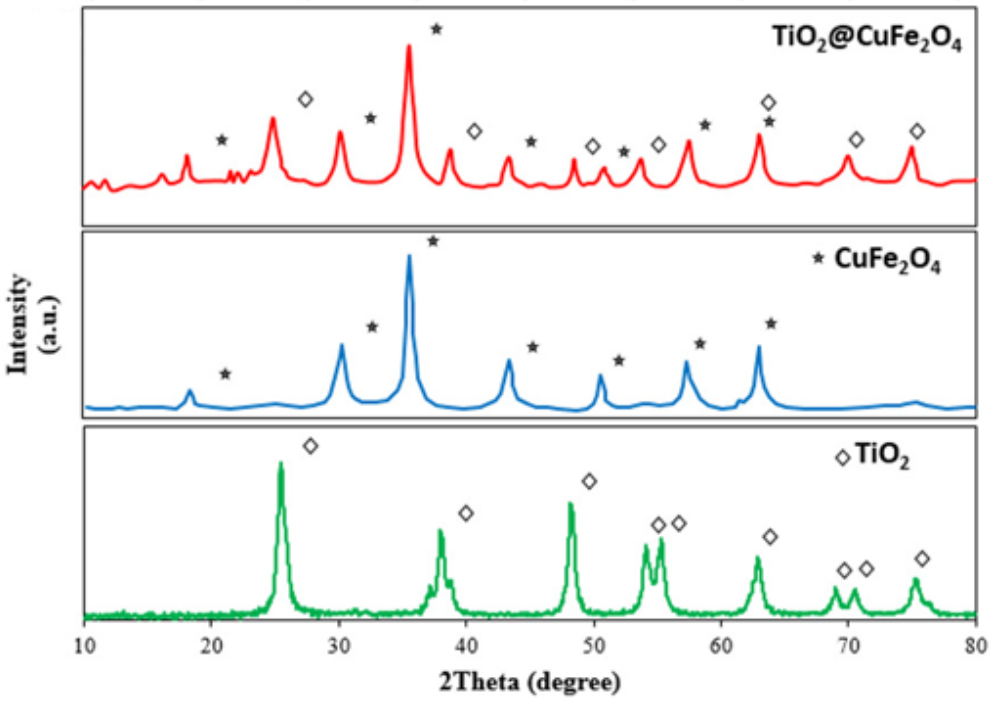

Figure 10. XRD patterns of neat TiO_2, neat $CuFe_2O_4$, and nanocomposite $TiO_2/CuFe_2O_4$ [109]. Republished with permission from Elsevier.

Figure 11a,b shows the SEM micrographs of $CuFe_2O_4$ and $TiO_2/CuFe_2O_4$, where the presence of agglomerated particles distributed randomly is apparent. The introduction of TiO_2 in the $CuFe_2O_4$ influenced the morphology of the nanocomposite $TiO_2/CuFe_2O_4$. The surface of the nanocomposite was much rougher than that of the $CuFe_2O_4$.

The TiO_2 agglomerated on the surface of $CuFe_2O_4$ can provide more active sites for the nanocomposite and improve its photocatalytic activity during organic pollutants degradation [109].

Several studies have reported the photocatalytic activity of copper ferrite and its nanocomposites in water and wastewater treatment [109,111,112].

For instance, a study done by Anandan et al. [110] reported good performance of magnetic $CuFe_2O_4$ as photocatalyst for the degradation of methylene blue (MB) dye in the presence of peroxydisulphate under UV–vis light.

The activity of the copper ferrite was attributed to the effect of the peroxydisulphate in the photocatalyst, which improved the photocatalytic degradation of methylene blue (95%) 75 min. Before the addition of the oxidant peroxydisulphate to the cobalt ferrite, the nanoparticles showed 16% MB dye degradation in 75 min.

A recent study conducted by Janani et al. [113] evaluated the magnetic nanocomposite $ZnO/CuFe_2O_4$ as a catalyst for methylene blue dye degradation under visible light. In their study, they demonstrated that the $ZnO/CuFe_2O_4$ photocatalyst was efficient in the degradation of methylene blue dye (86%) in 77 min.

The authors associated the activity of the nanocomposites with the hydroxyl radicals and holes generated, which play a principal role in the degradation of the dye. Furthermore, the photocatalyst also remained stable after six cycles of reuse. More studies on the activity

of copper ferrite nanocomposites for the degradation of organic pollutants are listed in Table 2.

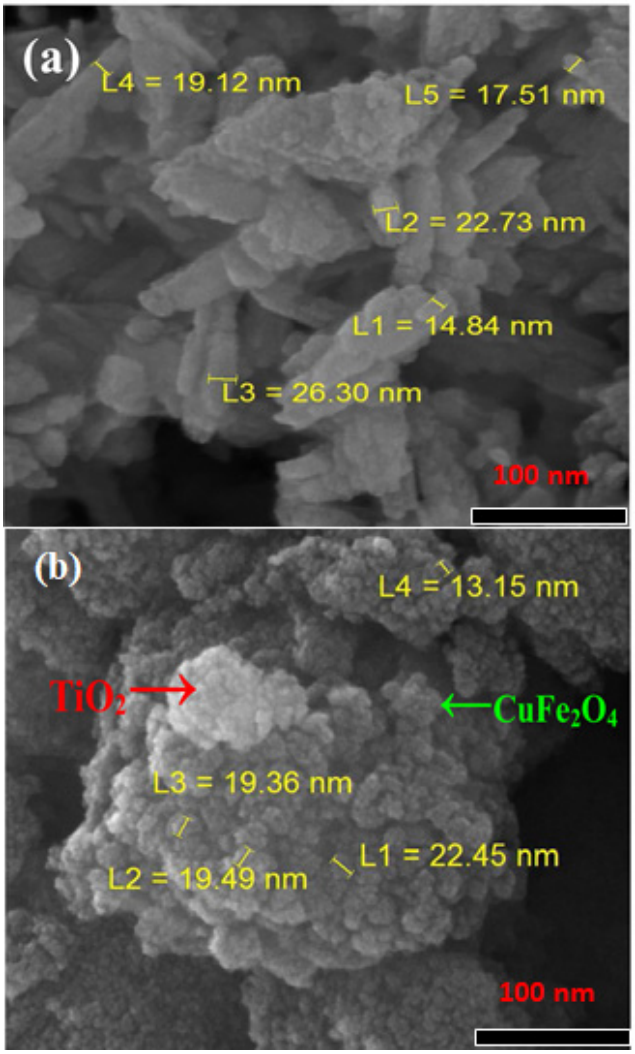

Figure 11. SEM micrographs of: (**a**) $CuFe_2O_4$ and (**b**) magnetic nanocomposite $TiO_2/CuFe_2O_4$ [109]. Republished with permission from Elsevier.

3.6. Mixed-Metal Ferrites and Nanocomposites

The introduction of different cations in the spinel ferrite system is required to improve the physicochemical properties of spinel ferrites. For instance, the substitution of magnetic cations such as Mn^{2+}, Ni^{2+}, Co^{2+}, and $Cu^{2+,}$ and diamagnetic ions such as Zn^{2+} and $Cd^{2+,}$ in spinel ferrites systems, changes the structural, morphological, opto-magnetic, and catalytic properties [114,115]. In general, this is attributed to the distribution of metallic ions in the tetrahedral and octahedral sites [115,116].

Ciocarlan et al. [117] evaluated the structural, morphological, and photocatalytic properties of magnetic nanoparticles $Co_{0.5}Zn_{0.25}M_{0.25}Fe_2O_4/TiO_2$, where *M* represent Ni^{2+}, Cu^{2+}, and Mn^{2+} ions. XRD patterns for TiO_2-based magnetic nanocomposites showed that the introduction of TiO_2 into the magnetic nanoparticles affected their structural properties (Figure 12).

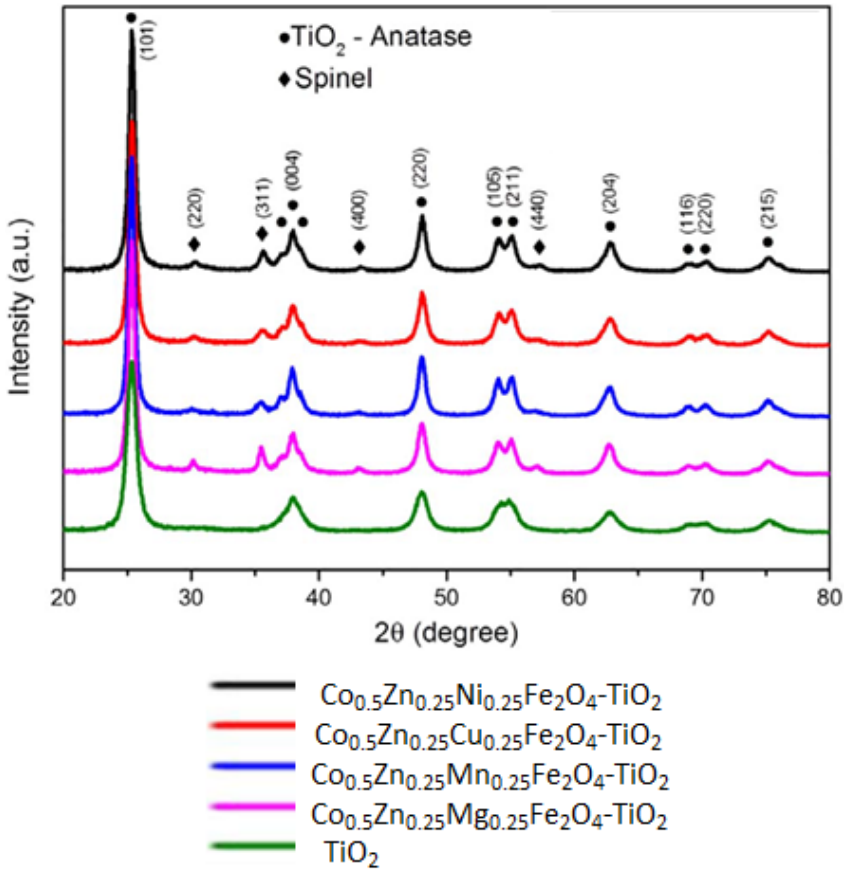

Figure 12. XRD pattern of TiO_2 and magnetic ferrite-based TiO_2 nanocomposites [117]. Republished with permission from Elsevier.

TEM micrographs for the two magnetic nanocomposites revealed variations in morphology upon substitution of M^{2+} cations (Ni^{2+} and Cu^{2+}) and introduction of TiO_2 to the $Co_{0.5}Zn_{0.25}M_{0.25}Fe_2O_4$ system (Figure 13).

Finally, in terms of photocatalytic activity, the results demonstrated that approximately 80% and 75% of methylene orange (MO) and methylene blue (MB) were effectively degraded by $Co_{0.5}Zn_{0.25}Ni_{0.25}Fe_2O_4/TiO_2$. The authors attributed the good photocatalytic activity to the Ni^{2+} ions and synergistic effect in combination with Co^{2+} ions [117].

Several other studies have also demonstrated the photocatalytic performance of complex-structured magnetic nanocomposites. For example, a $Mn_{1-x}Ni_xFe_2O_4$ catalyst with varying concentrations of nickel (x = 0.1, 0.2, 0.3, 0.4, and 0.5) was evaluated for indigo carmine dye degradation by Jesudoss et al. [118].

Amongst the obtained photocatalysts, the $Mn_{0.5}Ni_{0.5}Fe_2O_4$ catalyst exhibited higher photocatalytic performance in the degradation of indigo carmine dye, with 96% degradation within a 180 min period.

The material exhibited excellent saturation magnetization of 35.0 emu/g, demonstrating that this can be recoverable after a catalytic reaction. The authors concluded that the concentration of Ni^{2+} ions affected the structure of $MnFe_2O_4$, and that a high concentration of nickel ions reduced the crystallite size and increased the surface area, thereby affecting photocatalytic activity (Figure 14).

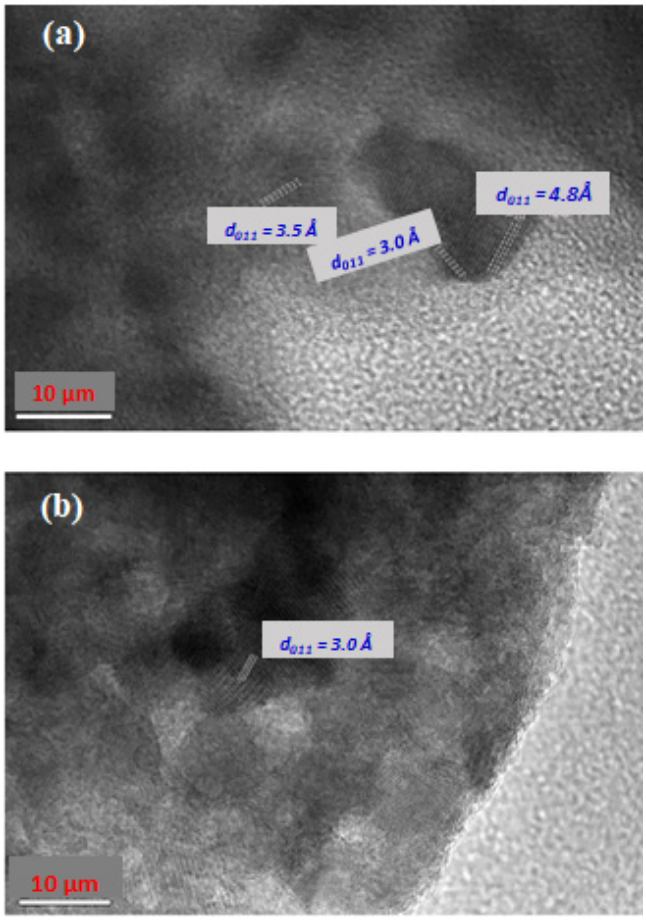

Figure 13. TEM images of the magnetic nanocomposites: (**a**) $Co_{0.5}Zn_{0.25}Ni_{0.25}Fe_2O_4/TiO_2$ and (**b**) $Co_{0.5}Zn_{0.25}Cu_{0.25}Fe_2O_4/TiO_2$ [117]. d_{011} demonstrates the different of diameter of particles. Republished with permission from Elsevier.

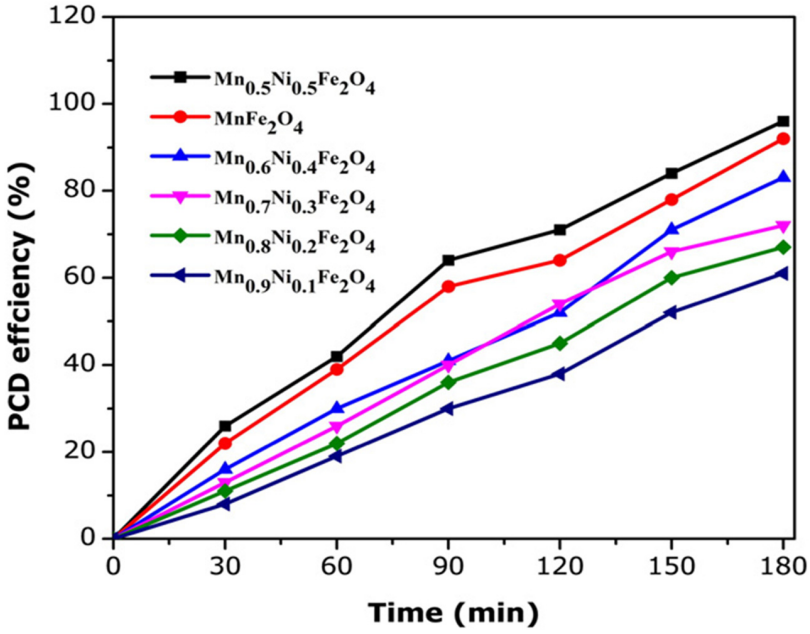

Figure 14. Effect of Ni^{2+} ions doped $MnFe_2O_4$ magnetic nanoparticles on the photocatalytic degradation (PCD) efficiency. The conditions used were IC = 150 mg/L, photocatalyst = 50 mg/100 mL, and λ = 365 nm) [118]. Republished with permission from Elsevier.

A study by Naik et al. [119] evaluated the performance of nanostructured zinc-doped cobalt ferrites ($Zn_xCo_{1-x}Fe_2O_4$ with (x = 0.0 to 0.6 with the step of 0.2) in the photocatalytic degradation of Congo Red (CR) and Evans Blue (EB) dyes. They established that the photocatalytic performance of cobalt ferrite increased with an increase in Zn-doping up to x = 0.4 then decreased thereafter (Figure 15).

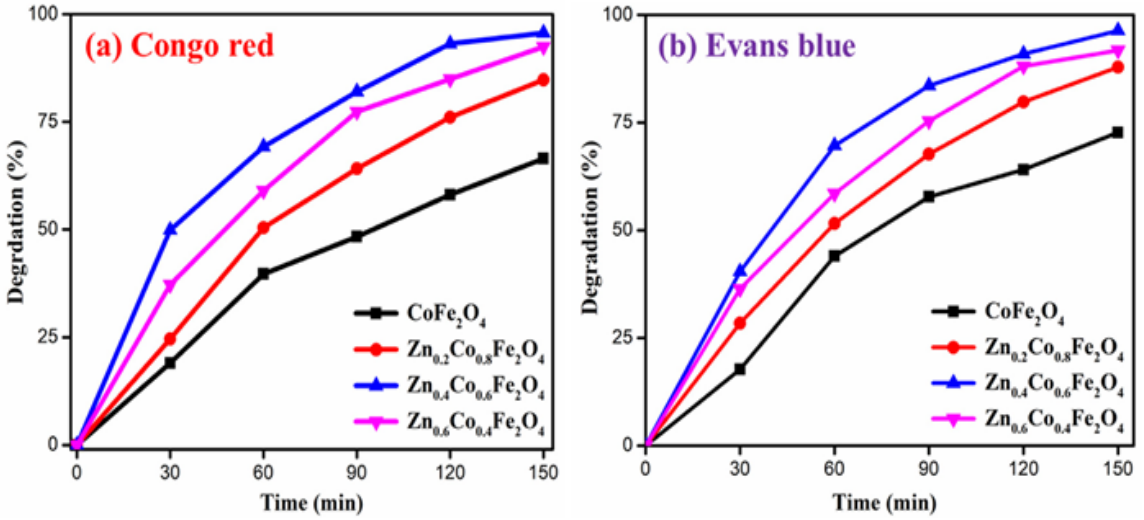

Figure 15. Photocatalytic results of: (**a**) Congo Red (CR) and (**b**) Evans Blue (EB) dyes using zinc-doped cobalt nanoparticles [119]. Republished with permission from Elsevier.

Additional studies revealed that higher Zn^{2+} doping concentrations increased the bactericidal properties of the $CoFe_2O_4$ towards human pathogens. For both Congo red (CR) and Evans Blue (EB) dyes, $Zn_{0.4}Co_{0.6}Fe_2O_4$ nanoparticles showed good photocatalytic activity in 150 min of irradiation time.

The study suggests that the synthesized nanoparticles are suitable for photocatalytic applications. More studies of photocatalytic activity of mixed metal ferrites nanocomposites are summarized in Table 2.

Table 2. Previous studies showing the photocatalytic degradation of organic pollutants using magnetic ferrites and ferrites-based zinc oxide and titanium oxides nanocomposites.

Magnetic Nanoparticles (MNPs)	Organic Pollutants	Dye (mg/L)	Photocatalyst (mg/L)	Irradiation Time (min)	Irradiation Source	Degradation (%)	References
$NiFe_2O_4/TiO_2$	Methyl Orange				UV–Vis	90	[120]
$CoFe_2O_4$	Bromophenol Blue	50	25	24	n/A	2	[121] [a]
$CuFe_2O_4$	Bromophenol blue	50	25	24	n/A	48	[121]
$FeFe_2O_4$	Bromophenol blue	50	25	24	n/A	99	[121]
$MnFe_2O_4$	Bromophenol blue	50	25	24	n/A	0	[121]
$CoFe_2O_4$	Chicago Sky Blue	50	25	24	n/A	93	[121]
$CuFe_2O_4$	Chicago Sky Blue	50	25	24	n/A	95	[121]
$FeFe_2O_4$	Chicago Sky Blue	50	25	24	n/A	98	[121]
$MnFe_2O_4$	Chicago Sky Blue	50	25	24	n/A	91	[121]
$CoFe_2O_4$	Cu Phthalocyanine	50	25	24	n/A	70	[121]
$CuFe_2O_4$	Cu Phthalocyanine	50	25	24	n/A	75	[121]
$FeFe_2O_4$	Cu Phthalocyanine	50	25	24	n/A	92	[121]
$MnFe_2O_4$	Cu Phthalocyanine	50	25	24	n/A	19	[121]
$CoFe_2O_4$	Eosin Yellowish	50	25	24	n/A	25	[121]
$CuFe_2O_4$	Eosin Yellowish	50	25	24	n/A	53	[121]
$FeFe_2O_4$	Eosin Yellowish	50	25	24	n/A	85	[121]
$MnFe_2O_4$	Eosin Yellowish	50	25	24	n/A	12	[121]
$CoFe_2O_4$	Evans Blue	50	25	24	n/A	73	[121]
$CuFe_2O_4$	Evans Blue	50	25	24	n/A	92	[121]
$FeFe_2O_4$	Evans Blue	50	25	24	n/A	99	[121]
$MnFe_2O_4$	Evans Blue	50	25	24	n/A	8	[121]
$CoFe_2O_4$	Naphthol Blue Black	50	25	24	n/A	68	[121]
$CuFe_2O_4$	Naphthol Blue Black	50	25	24	n/A	95	[121]
$FeFe_2O_4$	Naphthol Blue Black	50	25	24	n/A	93	[121]
$MnFe_2O_4$	Naphthol Blue Black	50	25	24	n/A	75	[121]
$CoFe_2O_4$	Phenol Red	50	25	24	n/A	85	[121]
$CuFe_2O_4$	Phenol Red	50	25	24	n/A	86	[121]
$FeFe_2O_4$	Phenol Red	50	25	24	n/A	81	[121]
$MnFe_2O_4$	Phenol Red	50	25	24	n/A	63	[121]
$CoFe_2O_4$	Poly B-411	50	25	24	n/A	0	[121]
$CuFe_2O_4$	Poly B-411	50	25	24	n/A	7	[121]
$FeFe_2O_4$	Poly B-411	50	25	24	n/A	38	[121]
$MnFe_2O_4$	Poly B-411	50	25	24	n/A	0	[121]
$CoFe_2O_4$	Reactive Orange 16	50	25	24	n/A	21	[121]
$CuFe_2O_4$	Reactive Orange 16	50	25	24	n/A	86	[121]

Table 2. *Cont.*

Magnetic Nanoparticles (MNPs)	Organic Pollutants	Dye (mg/L)	Photocatalyst (mg/L)	Irradiation Time (min)	Irradiation Source	Degradation (%)	References
$FeFe_2O_4$	Reactive Orange 16	50	25	24	n/A	77	[121]
$MnFe_2O_4$	Reactive Orange 16	50	25	24	n/A	6	[121]
$CuFe_2O_4$	4-chlorophenol	200	30	30	UV–Vis	81	[115]
$CuFe_2O_4$-TiO_2	4-chlorophenol	200	30	30	UV–Vis	84	[115]
$Cu_{0.9}Mn_{0.1}Fe_2O_4/TiO_2$	4-chlorophenol	200	30	30	UV–Vis	88	[115]
$Cu_{0.8}Mn_{0.2}Fe_2O_4/TiO_2$	4-chlorophenol	200	30	30	UV–Vis	92	[115]
$Cu_{0.7}Mn_{0.3}Fe_2O_4/TiO_2$	4-chlorophenol	200	30	30	UV–Vis	94	[115]
$Cu_{0.6}Mn_{0.4}Fe_2O_4/TiO_2$	4-chlorophenol	200	30	30	UV–Vis	96	[115]
$Cu_{0.5}Mn_{0.5}Fe_2O_4/TiO_2$	4-chlorophenol	200	30	30	UV–Vis	98	[115]
$(Co,Mn)Fe_2O_4@TiO_2$	Azo dye	10	10	960	UV	76	[122]
$ZnFe_2O_4$	Rhodamine B	10	20	150	200–700 nm	60	[123]
$TiO_2/ZnFe_2O_4$	Rhodamine B	9.6	10	150	λ = 254 nm	99.7	[124]
$TiO_2/ZnFe_2O_4$ (1:1)	Rhodamine B	n/A	n/A	150	UV	47	[125]
$TiO_2/ZnFe_2O_4$ (2:1)	Rhodamine B	n/A	n/A	150	UV	58	[125]
$TiO_2/ZnFe_2O_4$ (3:1)	Rhodamine B	n/A	n/A	150	UV	87	[125]
$TiO_2/ZnFe_2O_4$ (4:1)	Rhodamine B	n/A	n/A	150	UV	95	[125]
$ZnFe_2O_4$	Rhodamine B	20	80	300	UV–Vis	38.4	[126]
$ZnFe_2O_4$ nanospheres	Rhodamine B	20	80	300	UV–Vis	100	[126]
$ZnFe_2O_4$	Rhodamine B	20	500	360	UV-light	45	[86]
$ZnFe_2O_4$ [b]	Rhodamine B	20	500	360	UV-light	88	[86]
$ZnFe_2O_4$ [c]	Rhodamine B	20	500	360	UV-light	75	[86]
$ZnFe_2O_4$ [d]	Rhodamine B	20	500	360	UV-light	60	[86]
$ZnFe_2O_4$ [b]	Rhodamine B	20	500	360	Dark	0	[86]
$TiO_2/CoFe_2O_4$ (10%)	Methylene Blue	5	0.5	60	UV	56	[127]
$TiO_2/CoFe_2O_4$ (20%)	Methylene Blue	5	0.5	60	UV	60	[127]
$TiO_2/CoFe_2O_4$ (30%)	Methylene Blue	5	0.5	60	UV	57	[127]
TiO_2/Ni-Cu-Zn ferrite	Methylene Blue	20	13	120	UV	82	[128]
TiO_2/Ni-Cu-Zn ferrite	Methylene Blue	20	20	120	UV	98	[128]
TiO_2/Ni-Cu-Zn ferrite	Methylene Blue	20	26	120	UV	99	[128]
TiO_2/Ni-Cu-Zn ferrite	Methylene Blue	20	33	120	UV	95	[128]
$ZnFe_2O_4$	Methylene Blue	10	6	180	UV	28	[129]
$MnFe_2O_4$ [e]	Methylene Blue	7	300	1200	Visible light	15.2	[92]
$MnFe_2O_4$ [f]	Methylene Blue	7	300	1200	Visible light	67.2	[92]
$ZnFe_2O_4$	Methylene Blue	10	100	360	UV–Vis	8	[130]
$ZnFe_2O_4 + H_2O_2$	Methylene Blue	10	100	360	UV–Vis	52	[130]

Table 2. *Cont.*

Magnetic Nanoparticles (MNPs)	Organic Pollutants	Dye (mg/L)	Photocatalyst (mg/L)	Irradiation Time (min)	Irradiation Source	Degradation (%)	References
$ZnFe_2O_4 + H_2O_2$	Methylene Blue	10	100	360	Dark	45	[130]
TiO_2(57%)/$CoFe_2O_4$ (37%)	Methyl Orange	6	n/A	250	UV	0	[114]
TiO_2(62%)/$CoFe_2O_4$ (30%)	Methyl Orange	6	n/A	250	UV	25	[114]
$CoFe_2O_4$/ZnO	Methyl Orange	50	30	300	UV	93.9	[114]
$TiO_2/ZnFe_2O_4$	Methyl Orange	8	80	420	UV	80	[131]
$TiO_2/ZnFe_2O_4$ [g]	Methyl Orange	10	50	180	UV–Vis	5	[87]
$TiO_2/ZnFe_2O_4$ [h]	Methyl Orange	10	50	180	UV–Vis	13	[87]
$TiO_2/ZnFe_2O_4$ [i]	Methyl Orange	10	50	180	UV–Vis	27	[87]
$TiO_2/ZnFe_2O_4$ (0.15%)	Methyl Orange	25	5	240	UV–Vis	65	[132]
$TiO_2/ZnFe_2O_4$ (0.30%)	Methyl Orange	25	5	240	UV–Vis	75	[132]
$TiO_2/ZnFe_2O_4$ (1.5%)	Methyl Orange	25	5	240	UV–Vis	84	[132]
$TiO_2/ZnFe_2O_4$ (3.0%)	Methyl Orange	25	5	240	UV–Vis	73	[132]
$TiO_2/ZnFe_2O_4$ (6.05%)	Methyl Orange	25	5	240	UV–Vis	55	[132]
$ZnFe_2O_4$	Methyl Orange	25	5	240	UV–Vis	4	[132]
$ZnFe_2O_4$	Methyl Orange	10	4	60	UV-light	75	[133]
$ZnFe_2O_4$	Methyl Orange	10	100	240	UV–Vis	5	[134]
$TiO_2/ZnFe_2O_4$	Methyl Orange	10	100	240	UV–Vis	40	[134]
$TiO_2/ZnFe_2O_4$ (1.5%)	Methyl Orange	10	100	240	UV–Vis	12	[134]
$TiO_2/ZnFe_2O_4$ (3.0%)	Methyl Orange	10	100	240	UV–Vis	34	[134]
$TiO_2/ZnFe_2O_4$ (4.5%)	Methyl Orange	10	100	240	UV–Vis	24	[134]
$TiO_2/ZnFe_2O_4$ (6.0%)	Methyl Orange	10	100	240	UV–Vis	18	[134]
$CuFe_2O_4$-TiO_2	Methylene Blue	50	1000	180	UV–Vis	83.7	[135]
$ZnFe_2O_4$/ZnO	Methylene Blue	20	1000	360	UV	90	[136]
$ZnFe_2O_4$/ZnO	Remazol Brilliant Blue	20	1000	360	UV	100	[136]
$CoFe_2O_4 + H_2O_2$	Rhodamine B	10	100	270	UV-Vis	90.6	[137]
$CuFe_2O_4$-TiO_2	Methylene Blue	12	100	150	UV-Vis	47	[111]

[a] The reactions of various dyes were evaluated with ferrites and H_2O_2 with no applied irradiation [121]. [b] 9 nm average crystal size. [c] 14 nm average crystal size. [d] 19 nm average crystal size. [e] Thermal preparation. [f] Seed-hydrothermal preparation. [g] Prepared by citrate–nitrate method. [h] Prepared by thermal method. [i] Prepared by thermal method, recovered, and sintered at 800 °C.

It is important to note that, besides the focus of the development of magnetic nanocomposites for water and wastewater treatment, new recent trend of development of new materials is emerging. For example, Mir et al. [138] studied how confining AuNPs in a porous Si template can significantly enhance the photocatalytic activity of MO. The pores prevent agglomeration of nanoparticles and eliminate the need for any functionalization. Confinement of the AuNPs in the Si nanocavities prevents electron–hole recombination and facilitates the transfer of hot carriers from the Si support to accelerate the photocatalytic efficiency.

The results showed that the recyclable, low-band gap photocatalytic system has economic and environmental advantages that promote implementation of catalytic and separation processes in continuous flow mode, with the advantages associated with easier phase separation and product recovery, enhanced safety, and easier operation [138].

Another recent trend of study explored functional elastomeric copolymer membranes designed by nanoarchitectonics approach for Methylene Blue Removal. The results demonstrated specific adsorption abilities up to 18 mg/g of grafted cyclodextrins [139].

The findings obtained in these studies show that more studies can be explored in order to develop new nanomaterials that are sustainable and safer for water and wastewater applications.

4. Factors Affecting the Photocatalytic Activity of Magnetic Nanocomposites

The photocatalytic activity of magnetic nanocomposites is dependent on several factors such as surface area, concentrations of dopant metal ions, pH, and catalyst loading.

4.1. Catalyst Surface Area

Nanomaterials with a high specific surface area exhibit enhanced catalytic activity. A decrease in particle size takes one to the increase of the surface area, which improves the dispersion of the nanomaterials in solution. This results in an enhanced photon absorbance, leading to the retrieval of their photocatalytic performance [140–143].

A study done by Padmapriya et al. [144] evaluated the effect of surface areas of magnetic nanoparticles system $Ni_xZn_{1-x}Fe_2O_4$, with different concentrations of Ni^{2+} ions ($0.0 \leq x \leq 1.0$) in photocatalytic degradation of methylene blue dye (Figure 16a).

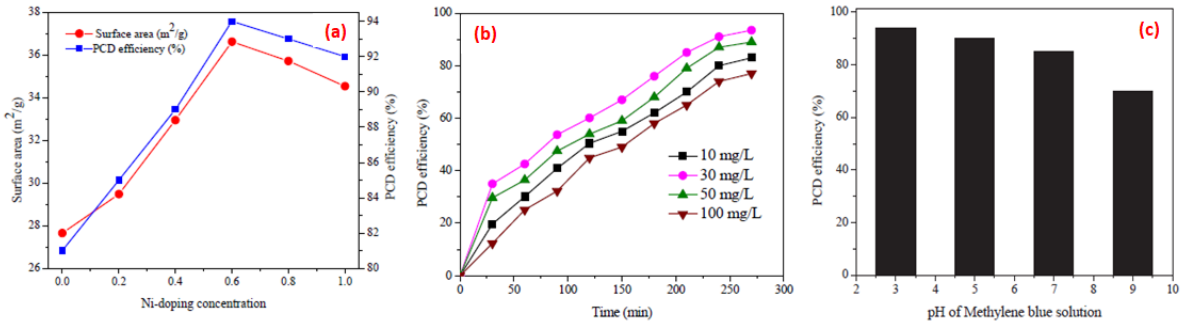

Figure 16. (**a**) Effect of surface area for photocatalytic degradation efficiency of spinel $Ni_xZn_{1-x}Fe_2O_4$ (x = 0.0, 0.2, 0.4, 0.6, 0.8, and 1.0) nanoparticles. (**b**) Effect of catalyst amount on the photocatalytic degradation (PCD) efficiency of spinel $Ni_{0.6}Zn_{0.4}Fe_2O_4$ nanoparticles. (**c**) Effect of pH on photodegradation of methylene blue using catalyst $Ni_{0.6}Zn_{0.4}Fe_2O_4$ [144]. Republished with permission from Elsevier.

The results demonstrated that better photocatalytic activity was found for the nanocatalyst $Ni_{0.6}Zn_{0.4}Fe_2O_4$, which had a high surface area (36.6 m^2/g) compared to the other samples. It can be understood from this study that surface area is also related to the active sites on the catalytic surface, which enhance the photocatalytic activity.

Manikandan et al. [115] demonstrated that the photocatalytic degradation of 4-Chlorophenol (4-CP) using the photocatalyst $ZnFe_2O_4$ was affected by the particle size and morphology of the catalyst.

Additionally, a study conducted by Jia et al. [145] reported that the photocatalytic activity of $ZnFe_2O_4$ nanoparticles for methylene blue dye degradation was related to the surface properties and surface defects of the photocatalyst.

4.2. Effect of Catalyst Amount

The efficiency photocatalytic reactions can be influenced by the amount of the catalyst used. Padmapriya et al. [144] reported that the photocatalytic degradation of methylene blue dye was found to increase with an increase in the amount of the magnetic catalyst $Ni_{0.6}Zn_{0.4}Fe_2O_4$ until a certain amount of nanocatalyst loading (Figure 16b).

However, further increase in the catalyst loading demonstrated negative influence of the degradation plateaued. The authors also reported that adding an amount of the magnetic nanocatalyst increased the active sites on the catalyst surface, which in turn increased the amount of •OH (hydroxyl) and $\bullet O_2^-$ (superoxide) radicals and degraded the methylene blue (MB) dye.

Furthermore, the excess of amount of nanocatalyst beyond the optimum may have resulted in the agglomeration of catalyst particles and generated turbidity, which resulted in the decrease of the photocatalytic degradation efficiency [140,142,146].

4.3. Effect of pH

Generally, the solution pH is an important variable in water and wastewater treatment as it has a significant influence on the photocatalytic degradation process of organic compounds [10]. The variation of pH alters the surface charge of heterogeneous catalysts and, consequently, changes the photocatalytic activity of catalyst [147,148].

Figure 16c shows the influence of different pH (3, 4, 5, 6, 7, 8, and 9) on the photodegradation of methylene blue using the nanomagnetic catalyst $Ni_{0.6}Zn_{0.4}Fe_2O_4$ in a study conducted by Padmapriya et al. [144]. The results from this study showed that high photocatalytic degradation efficiency was achieved at pH = 3, due to electrostatic attraction between the anionic dye (MB) and the positively charged surface of nanocatalyst.

The authors demonstrated that at pH values above 7, the nanocatalyst surface became negatively charged, leading to electrostatic repulsion between the methylene blue dye and the catalyst, which reduced the photocatalytic degradation efficiency. More studies demonstrating the same behavior were reported by Mirkhani et al. [149] and Suwarnkar et al. [150].

5. Reusability of the Magnetic Nanocatalyst

Heterogeneous photocatalysis technology is always looking for an ideal photocatalyst, one that is reusable and that possesses high photocatalytic efficiency, a large specific surface area, and ability to absorb visible light [138]. Thus, the recyclability of catalysts is one of the key steps towards the sustainable application of photocatalysts and development of heterogeneous photocatalysis technology for water and wastewater treatment. The recyclability of catalysts is also related to their actual operational costs.

Recently, several studies have demonstrated satisfactory recyclability of nanomagnetic nanoparticles via magnetic separation processes using a magnetic field [5,10,150–152].

Krishna et al. [100] reported the reusability of the $CoFe_2O_4/TiO_2$ nanocatalysts for acid blue 113 (AB113) dye degradation through magnetic separation where its photocatalytic activity was found to be retained up to six consecutive cycles and without considerable loss of photocatalytic activity and stability (Figure 17).

Table 3 shows additional results of the activities of reused magnetic nanocomposites for organic photodegradation processes. Most of the magnetic nanocomposites are recyclable up to more than three runs, demonstrating their stability during their application for water and wastewater treatment for organic pollutants removal. Therefore, these studies are indicators for possible industrial or large-scale application.

Table 3. Reusability of magnetic nanoparticles (MNPs) for organic pollutants degradation.

Magnetic Nanocomposites	Organic Pollutants	Dye (mg/L)	Photocatalyst (g/L)	Irradiation Time (min)	pH	Cycles of Reusability of MNPs	Degradation Efficiency (%)	Irradiation Source	References
$CoFe_2O_4/TiO_2$-SiO_2	Methylene blue dye	0.3	0.33	30	6	6	93.2	UV	[10]
$NiFe_2O_4$	Reactive blue 5	0.05	0.03	10	1–11	4	85.0	n/A	[83]
$NiFe_2O_4/ZnO$	Congo red (CR)	0.02	0.05	40	5.5	5	97.0	UV–Vis	[16]
$CoFe_2O_4/ZnO$	Methylene blue dye	5	0.025	60	n/A	3	-	UV–Vis	[5]
$CoFe_2O_4/TiO_2$	Methylene blue dye	n/A	n/A	360	n/A	5	93.8	UV	[153]
$ZnFe_2O_4/TiO_2/Cu$	Naproxen	0.03	0.1	120	4–9	5	72.3	Sunlight	[154]
$ZnFe_2O_4/TiO_2$	Rhodamine B	10	1	30	3–11	5	>99	UV–Vis	[155]
$CoFe_2O_4/TiO_2/rGO$	Chlorpyrifos	5	0.4	60	5.8	8	-	UV	[152]
$ZnFe_2O_4/TiO_2$	Methylene blue dye	20	0.05	360	5.6	5	93.2	UV–Vis	[151]
$ZnFe_2O_4/ZnO$	Methylene blue dye	n/A	0.1	120	n/A	3	-	UV	[17]
$NiFe_2O_4/TiO_2$	Methyl Orange	10	1	300	9.5–10	3	-	Visible light	[156]
$Cu_{0.5}Mn_{0.5}Fe_2O_4/TiO_2$	4-chlorophenol	30	0.2	300	8	5	98.0	UV	[115]
$ZnO/MnFe_2O_4$	Methylene blue dye	n/A	n/A	300	3–9	6	86.0	UV–Vis	[113]
$CuFe_2O_4/TiO_2$	Methylene blue dye	30	1	120	2.2	3	81.2	UV–Vis	[135]
$ZnFe_2O_4/ZnO$	Methylene blue dye	10	0.1	200	9–10	3	79.0	UV	[85]
$MnFe_2O_4/TiO_2$-rGO	Ciprofloxacin	30	0.06	300	1–6	6	75.0	UV–Vis	[106]
$ZnFe_2O_4/TiO_2$	Bisphenol A	10	1	300	9.5–10	5	>90	UV–Vis	[157]

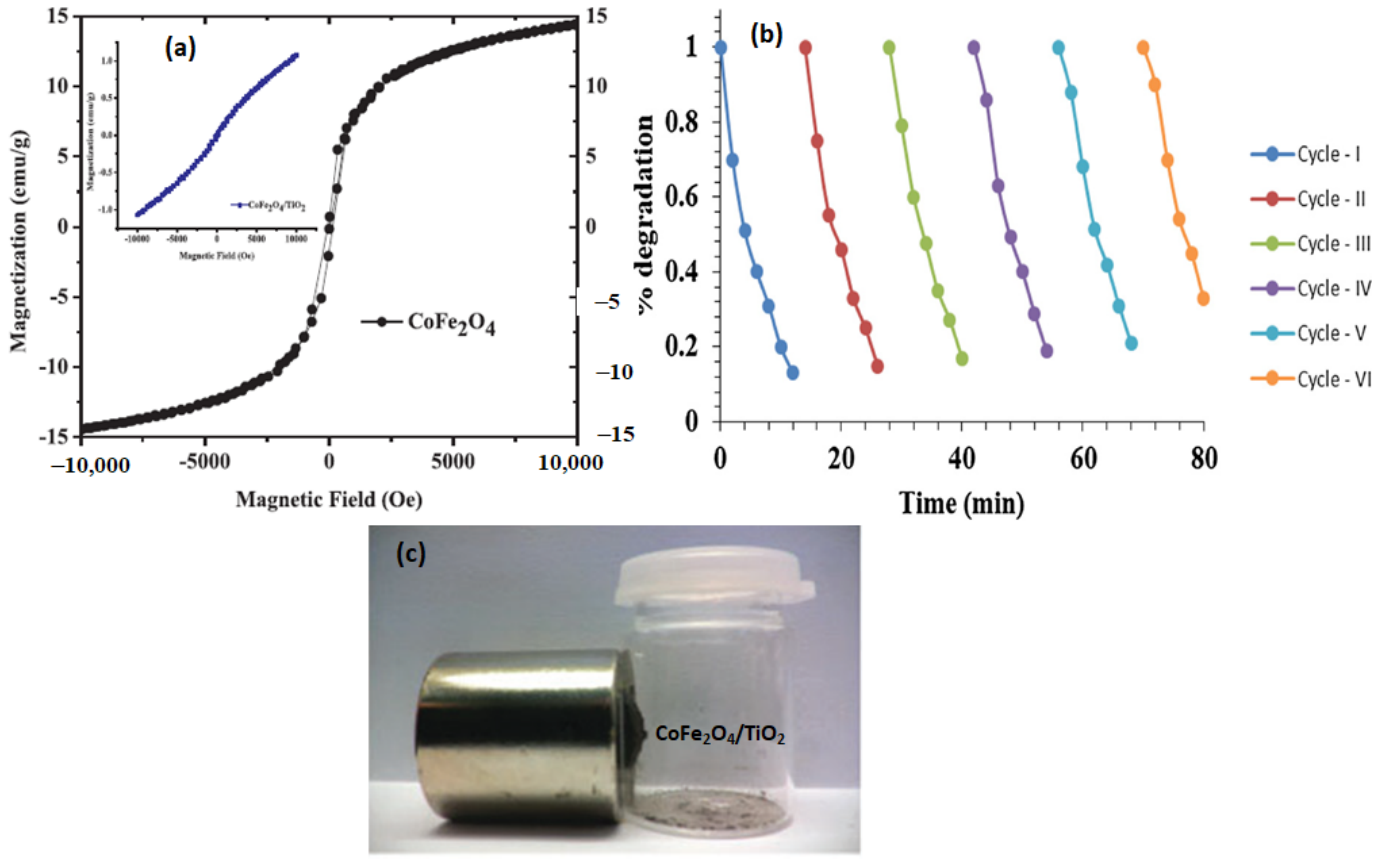

Figure 17. (**a**) Magnetization hysteresis loops observed for the $CoFe_2O_4$ (black dots) and $CoFe_2O_4/TiO_2$ nanocatalysts (blue line) [100]; (**b**) photocatalytic degradation of AB113 in the presence of magnetically recyclable $CoFe_2O_4/TiO_2$ nanocatalysts in cycles [100]; and (**c**) magnetic responsiveness of $CoFe_2O_4/TiO_2$ with an external magnetic field [153]. Republished with permission from Elsevier.

6. The Overlooked Social Dimension

The focus of most water and wastewater-related research has been on the technical aspects of the problem and improvements in terms of water quality and in minimizing environmental and health impacts, with very limited attention to its basic social and cultural sustainability dimensions [158].

A study done by Wichelns et al. [159] demonstrated that there is a need for a paradigm shift from the 'treatment for disposal' to the 'treatment for reuse' since wastewater contains pollutants such as organic and inorganic compounds which may pose health risks if not well managed [159].

Additionally, even when wastewater is treated using advanced technologies and health risks are carefully addressed and controlled, irrespective of all scientific evidence, the social perception remains the driver of the success or failure of wastewater reuse schemes [158].

Depending on public perceptions, impressions, and attitudes, the development of a wastewater scheme can be supported or constrained. Negative public perception can prevent well-planned projects from moving forward. On the other hand, positive public perception, which leads to greater acceptance, is the key element for the successful implementation of wastewater treatment [159,160].

Saad et al. [158] reported that various local communities around the world have rejected several water and wastewater treatment projects by their governments due to inadequate community consultation which resulted in negative public perception.

In summary, it can be said that recognizing the role of the social base for wastewater management from risk reduction to reuse can have major implications, for example, on the choice and effectiveness of the technologies employed.

Added to this is the creation of economic incentives for the public and private sector institutions to invest in sanitation and to generate income for private operators as well as secure their sustainability [161].

7. Conclusions and Recommendation

The development and application of magnetic ferrite-based titanium oxide and zinc oxide nanocomposite as catalysts are extremely promising for the removal of organic pollutants from water and wastewater, as shown by various studies presented in this review. Studies demonstrated that these catalysts can be prepared by different methods such as sol-gel, co-precipitation, hydrothermal, and combustion. However, the methods of synthesis are chosen based on their advantages. The magnetic nanoparticles (MNPs) have several advantages, including that they are easily separated by an external magnetic field without loss of the nanocatalyst, which can be reused up to several runs of experiments. In most of studies, the magnetic based titanium oxide and zinc oxide nanocomposite exhibited an excellent catalytic activity for organic pollutants removal. Additionally, some studies showed that these catalysts were even effective after more three successive cycling runs. The catalytic activity of the MNPs as catalysts is a direct outcome of its intrinsic characteristics as well as of its synthesis method; nevertheless, the catalytic performance can be influenced by conditions that are imposed on these materials to prepare them for a given application. Additionally, the method of synthesis plays a principal role in the physicochemical properties of the catalyst obtained. However, the synthesis of magnetic nanoparticles and their relevance for organic dyes removal from water and wastewater still require more investigation in order to achieve the optimum optimization for large-scale for subsequent practical applications. Finally, studies of the application of MNPs-based oxides nanocomposites in water and wastewater treatment are still few; however, more studies are still required. Additionally, with this technology in progress, scientists have enough supporting theory to upscale and provide a cleaner environment and safe drinking water to human populations.

Author Contributions: Conceptualization, A.B.M.; writing—original draft preparation, A.B.M.; writing—review and editing, A.B.M., W.M., J.L.A., and S.T.; supervision, A.B.M. and S.T.; project administration, S.T. and W.M.; funding acquisition, S.T. and W.M. All authors have read and agreed to the published version of the manuscript.

Funding: No funding grant was used for this work.

Data Availability Statement: Data sharing not applicable—no new data generated.

Acknowledgments: The authors thank the Department of Chemical Engineering, University of Pretoria, and Department of Chemical, Metallurgical and Materials, Tshwane University of Technology South Africa for all the technical and logistical support.

Conflicts of Interest: The authors declare no conflict of interest.

Abbreviations

AB113	Acid Blue 113
CR	Congo Red
4-CP	4-Chlorophenol
DSC	Differential Scanning Calorimetry
EB	Evans Blue
Ms	Saturation Magnetization

MNPs	Magnetic Nanoparticles
MB	Methylene Blue
MO	Methylene Orange
MG	Malachite Green
RB5	Reactive Blue 5
SEM	Scanning Electron Microscopy
TGA	Thermogravimetric Analysis
TEM	Transmission Electron Microscopy
T_C	Curie Temperature
UV	Ultraviolet
VSM	Vibrating Sample Magnetometer
XRD	X-ray Diffraction

References

1. Liu, Y.; Sun, L.; Wu, J.; Fang, T.; Cai, R.; Wei, A. Preparation and photocatalytic activity of ZnO/Fe_2O_3 nanotube composites. *Mater. Sci. Eng. B* **2015**, *194*, 9–13. [CrossRef]
2. Cheng, M.; Zeng, G.; Huang, D.; Lai, C.; Xu, P.; Zhang, C.; Liu, Y. Hydroxyl radicals based advanced oxidation processes (AOPs) for remediation of soils contaminated with organic compounds: A review. *Chem. Eng. J.* **2016**, *284*, 582–598. [CrossRef]
3. Cahino, A.M.; Loureiro, R.G.; Dantas, J.; Madeira, V.S.; Fernandes, P.C.R. Characterization and evaluation of ZnO/CuO catalyst in the degradation of methylene blue using solar radiation. *Ceram. Int.* **2019**, *45*, 13628–13636. [CrossRef]
4. de Oliveira, P.L.; Lima, N.S.; de Melo Costa, A.C.F.; Cavalcanti, E.B.; de Sousa Conrado, L. Obtaining TiO_2: $CoFe_2O_4$ nanocatalyst by Pechini method for diuron degradation and mineralization. *Ceram. Int.* **2020**, *46*, 9421–9435. [CrossRef]
5. Wilson, A.; Mishra, S.R.; Gupta, R.; Ghosh, K. Preparation and photocatalytic properties of hybrid core–shell reusable $CoFe_2O_4$–ZnO nanospheres. *J. Magn. Magn. Mater.* **2012**, *324*, 2597–2601. [CrossRef]
6. Dette, C.; Pérez-Osorio, M.A.; Kley, C.S.; Punke, P.; Patrick, C.E.; Jacobson, P.; Giustino, F.; Jung, S.J.; Kern, K. TiO_2 anatase with a bandgap in the visible region. *Nano Lett.* **2014**, *14*, 6533–6538. [CrossRef] [PubMed]
7. Farhadi, A.; Mohammadi, M.R.; Ghorbani, M. On the assessment of photocatalytic activity and charge carrier mechanism of TiO_2@SnO_2 core-shell nanoparticles for water decontamination. *J. Photochem. Photobiol. A Chem.* **2017**, *338*, 171–177. [CrossRef]
8. Kazemi, M.; Mohammadizadeh, M.R. Simultaneous improvement of photocatalytic and superhydrophilicity properties of nano TiO_2 thin films. *Chem. Eng. Res. Des.* **2012**, *90*, 1473–1479. [CrossRef]
9. Ahmed, M.A.; El-Katori, E.E.; Gharni, Z.H. Photocatalytic degradation of methylene blue dye using Fe_2O_3/TiO_2 nanoparticles prepared by sol–gel method. *J. Alloys Compd.* **2013**, *553*, 19–29. [CrossRef]
10. Harraz, F.A.; Mohamed, R.M.; Rashad, M.M.; Wang, Y.C.; Sigmund, W. Magnetic nanocomposite based on titania–silica/cobalt ferrite for photocatalytic degradation of methylene blue dye. *Ceram. Int.* **2014**, *40*, 375–384. [CrossRef]
11. Gong, H.; Chu, W. Determination and toxicity evaluation of the generated products in sulfamethoxazole degradation by UV/$CoFe_2O_4$/TiO_2. *J. Hazard. Mater.* **2016**, *314*, 197–203. [CrossRef]
12. Mmelesi, O.K.; Masunga, N.; Kuvarega, A.; Nkambule, T.T.; Mamba, B.B.; Kefeni, K.K. Cobalt ferrite nanoparticles and nanocomposites: Photocatalytic, antimicrobial activity and toxicity in water treatment. *Mater. Sci. Semicond. Process.* **2021**, *123*, 105523. [CrossRef]
13. Sundararajan, R.; Srinivasan, V. Catalytic decomposition of nitrous oxide on $CuxCo_{3\_}xO_4$ spinels. *Appl. Catal.* **1991**, *73*, 165–171. [CrossRef]
14. Mapossa, A.B.; Dantas, J.; Silva, M.R.; Kiminami, R.H.; Costa, A.C.F.; Daramola, M.O. Catalytic performance of $NiFe_2O_4$ and $Ni_{0.3}Zn_{0.7}Fe_2O_4$ magnetic nanoparticles during biodiesel production. *Arab. J. Chem.* **2020**, *13*, 4462–4476. [CrossRef]
15. Hajalilou, A.; Mazlan, S.A. A review on preparation techniques for synthesis of nanocrystalline soft magnetic ferrites and investigation on the effects of microstructure features on magnetic properties. *Appl. Phys. A Mater. Sci. Process.* **2016**, *122*, 1–15. [CrossRef]
16. Zhu, H.Y.; Jiang, R.; Fu, Y.Q.; Li, R.R.; Yao, J.; Jiang, S.T. Novel multifunctional $NiFe_2O_4$/ZnO hybrids for dye removal by adsorption, photocatalysis and magnetic separation. *Appl. Surf. Sci.* **2016**, *369*, 1–10. [CrossRef]
17. Maynez-Navarro, O.D.; Mendez-Rojas, M.A.; Flores-Cervantes, D.X.; Kuri, U.S.; Sanchez-Salas, J.L. Recyclable and Photocatalytic Properties of $ZnFe_2O_4$/ZnO for Wastewater Treatment and Disinfection. *ChemistrySelect* **2020**, *5*, 15167–15174. [CrossRef]
18. Rahmayeni, R.A.; Stiadi, Y.; Jamarun, N.; Emriadi, A.S. Photocatalytic Performance of ZnO-$ZnFe_2O_4$ Magnetic Nanocomposites on Degradation of Congo Red Dye Under Solar Light Irradiation. *J. Mater. Environ. Sci.* **2017**, *8*, 1634–1643.
19. Reddy, D.H.K.; Yun, Y.S. Spinel ferrite magnetic adsorbents: Alternative future materials for water purification? *Coord. Chem. Rev.* **2016**, *315*, 90–111. [CrossRef]
20. Zhao, H.; Dong, Y.; Wang, G.; Jiang, P.; Zhang, J.; Wu, L.; Li, K. Novel magnetically separable nanomaterials for heterogeneous catalytic ozonation of phenol pollutant: $NiFe_2O_4$ and their performances. *Chem. Eng. J.* **2013**, *219*, 295–302. [CrossRef]
21. Andjelković, L.; Šuljagić, M.; Lakić, M.; Jeremić, D.; Vulić, P.; Nikolić, A.S. A study of the structural and morphological properties of Ni–ferrite, Zn–ferrite and Ni–Zn–ferrites functionalized with starch. *Ceram. Int.* **2018**, *44*, 14163–14168. [CrossRef]

22. Kefeni, K.K.; Mamba, B.B.; Msagati, T.A. Application of spinel ferrite nanoparticles in water and wastewater treatment: A review. *Sep. Purif. Technol.* **2017**, *188*, 399–422. [CrossRef]
23. Casbeer, E.; Sharma, V.K.; Li, X.Z. Synthesis and photocatalytic activity of ferrites under visible light: A review. *Sep. Purif. Technol.* **2012**, *87*, 1–14. [CrossRef]
24. Yuliantika, D.; Taufiq, A.; Hidayat, A.; Hidayat, N.; Soontaranon, S. Exploring structural properties of cobalt ferrite nanoparticles from natural sand. In *IOP Conference Series: Materials Science and Engineering*; IOP Publishing: Bristol, UK, 2019; Volume 515, p. 012047.
25. Narang, S.B.; Pubby, K. Nickel spinel ferrites: A review. *J. Magn. Magn. Mater.* **2021**, *519*, 167163. [CrossRef]
26. Hazra, S.; Ghosh, N.N. Preparation of nanoferrites and their applications. *J. Nanosci. Nanotechnol.* **2014**, *14*, 1983–2000. [CrossRef]
27. Amiri, G.R.; Yousefi, M.H.; Abolhassani, M.R.; Manouchehri, S.; Keshavarz, M.H.; Fatahian, S. Magnetic properties and microwave absorption in Ni–Zn and Mn–Zn ferrite nanoparticles synthesized by low-temperature solid-state reaction. *J. Magn. Magn. Mater.* **2011**, *323*, 730–734. [CrossRef]
28. Gupta, N.; Verma, A.; Kashyap, S.C. Micro structural, dielectric and magnetic behavior of spin deposited nanocrystalline nickel-zinc ferrite thin films for microwave applications. *J. Magn. Magn. Mater.* **2007**, *308*, 137–142. [CrossRef]
29. Liu, Y.; Li, J.; Min, F.; Zhu, J.; Zhang, M. Microwave-assisted synthesis and magnetic properties of $Ni_{1-x}ZnxFe_2O_4$ ferrite powder. *J. Magn. Magn. Mater.* **2014**, *354*, 295–298. [CrossRef]
30. Shafi, K.; Koltypin, Y.; Gedanken, A.; Prozorov, R.; Balogh, J.; Lendvai, J.; Felner, I. Sonochemical preparation of nano- sized amorphous $NiFe_2O_4$ particles. *J. Mater. Chem. Phys.* **1997**, *101*, 6409–6414.
31. Chen, D.H.; He, X.R. Synthesis of nickel ferrite nanoparticles by sol–gel method. *Mater. Res. Bull.* **2001**, *36*, 1369–1377. [CrossRef]
32. Zahi, S.; Hashim, M.; Daud, A.R. Synthesis, magnetic properties and microstructure of Ni–Zn ferrite by sol–gel technique. *J. Magn. Magn. Mater.* **2007**, *308*, 177–182. [CrossRef]
33. Atif, M.; Nadeem, M.; Grössinger, R.; Turtelli, R.S. Studies on the magnetic, magneto strictive and electrical properties of sol–gel synthesized Zn doped nickel ferrite. *J. Alloys Compd.* **2011**, *509*, 5720–5724. [CrossRef]
34. Kumar, S.J.; Prameela, P.; Rao, K.S.; Kiran, J.N.; Rao, K.H. Structural and Magnetic Properties of Copper-Substituted Nickel–Zinc Nanoparticles Prepared by Sol-Gel Method. *J. Supercond. Nov. Magn.* **2020**, *33*, 693–705. [CrossRef]
35. Yang, J.M.; Tsuo, W.J.; Yen, F.S. Preparation of ultrafine nickel ferrite powders using mixed Ni and Fe tartrates. *J. Solid State Chem.* **1999**, *145*, 50–57. [CrossRef]
36. Maaz, K.; Karim, S.; Mumtaz, A.; Hasanain, S.K.; Liu, J.; Duan, J.L. Synthesis and magnetic characterization of nickel ferrite nanoparticles prepared by co-precipitation route. *J. Magn. Magn. Mater.* **2009**, *321*, 1838–1842. [CrossRef]
37. Dantas, J.; Leal, E.; Mapossa, A.B.; Cornejo, D.R.; Costa, A.C.F.M. Magnetic nanocatalysts of $Ni_{0.5}Zn_{0.5}Fe_2O_4$ doped with Cu and performance evaluation in transesterification reaction for biodiesel production. *Fuel* **2017**, *191*, 463–471. [CrossRef]
38. Mapossa, A.B.; Dantas, J.; Diniz, V.C.S.; Silva, M.R.; Kiminami, R.H.G.A.; Costa, A.C.F.M. Síntese e caracterização do ferroespinélio $Ni_{0.7}Zn_{0.3}Fe_2O_4$: Avaliação de desempenho na esterificação metílica e etílica. *Cerâmica* **2017**, *63*, 223–232. [CrossRef]
39. Abbas, M.K.; Khan, M.A.; Mushtaq, F.; Warsi, M.F.; Sher, M.; Shakir, I.; AlyAboud, M.F. Impact of Dy on structural, dielectric and magnetic properties of Li-Tb-nanoferrites synthesized by micro-emulsion method. *Ceram. Int.* **2017**, *43*, 5524–5533. [CrossRef]
40. Rozman, M.; Drofenik, M. Hydrothermal synthesis of manganese zinc ferrites. *J. Am. Ceram. Soc.* **1995**, *78*, 2449–2455. [CrossRef]
41. Zhao, L.; Zhang, H.; Xing, Y.; Song, S.; Yu, S.; Shi, W.; Guo, X.; Yang, J.; Lei, Y.; Cao, F. Studies on the magnetism of cobalt ferrite nanocrystals synthesized by hydrothermal method. *J. Solid State Chem.* **2008**, *181*, 245–252. [CrossRef]
42. Nejati, K.; Zabihi, R. Preparation and magnetic properties of nano size nickel ferrite particles using hydrothermal method. *Chem. Cent. J.* **2012**, *6*, 23. [CrossRef] [PubMed]
43. Feng, J.; Su, L.; Ma, Y.; Ren, C.; Guo, Q.; Chen, X. $CuFe_2O_4$ magnetic nanoparticles: A simple and efficient catalyst for the reduction of nitrophenol. *Chem. Eng. J.* **2013**, *221*, 16–24. [CrossRef]
44. Chen, C.; Zuo, W.Q.; Yang, J.C.E.; Cui, H.J.; Fu, M.L. Yolk–shell structured $CoFe_2O_4$ microspheres as novel catalysts for peroxymonosulfate activation for efficient degradation of butyl paraben. *RSC Adv.* **2016**, *6*, 10136. [CrossRef]
45. George, M.; John, A.M.; Nair, S.S.; Joy, P.A.; Anantharaman, M.R. Finite size effects on the structural and magnetic properties of sol–gel synthesized $NiFe_2O_4$ powders. *J. Magn. Magn. Mater.* **2006**, *302*, 190–195. [CrossRef]
46. El-Okr, M.M.; Salem, M.A.; Salim, M.S.; El-Okr, R.M.; Ashoush, M.; Talaat, H.M. Synthesis of cobalt ferrite nano-particles and their magnetic characterization. *J. Magn. Magn. Mater.* **2011**, *323*, 920–926. [CrossRef]
47. Konecny, A.P.; Covarrubias, J.; Wang, H. Magnetic Nanoparticle Design and Application in Magnetic Hyperthermia. In *Magnetic Nanomaterials: Applications in Catalysis and Life Sciences*; Bossmann, S.H., Wang, H., Eds.; RSC: London, UK, 2017.
48. Ali, A.; Hira Zafar, M.Z.; Ul Haq, I.; Phull, A.R.; Ali, J.S.; Hussain, A. Synthesis, characterization, applications, and challenges of iron oxide nanoparticles. *Nanotechnol. Sci. Appl.* **2016**, *9*, 49. [CrossRef]
49. Gopalan Sibi, M.; Verma, D.; Kim, J. Magnetic core–shell nanocatalysts: Promising versatile catalysts for organic and photocatalytic reactions. *Catal. Rev.* **2020**, *62*, 163–311. [CrossRef]
50. Bhagwat, V.R.; Humbe, A.V.; More, S.D.; Jadhav, K.M. Sol-gel auto combustion synthesis and characterizations of cobalt ferrite nanoparticles: Different fuels approach. *Mater. Sci. Eng. B* **2019**, *248*, 114388. [CrossRef]
51. Venturini, J.; Zampiva, R.Y.S.; Arcaro, S.; Bergmann, C.P. Sol-gel synthesis of substoichiometric cobalt ferrite ($CoFe_2O_4$) spinels: Influence of additives on their stoichiometry and magnetic properties. *Ceram. Int.* **2018**, *44*, 12381–12388. [CrossRef]

52. Motavallian, P.; Abasht, B.; Abdollah-Pour, H. Zr doping dependence of structural and magnetic properties of cobalt ferrite synthesized by sol–gel based Pechini method. *J. Magn. Magn. Mater.* **2018**, *451*, 577–586. [CrossRef]
53. Hossain, M.S.; Alam, M.B.; Shahjahan, M.; Begum, M.H.A.; Hossain, M.M.; Islam, S.; Khatun, N.; Hossain, M.; Alam, M.S.; Al-Mamun, M. Synthesis, structural investigation, dielectric and magnetic properties of Zn^{2+}-doped cobalt ferrite by the sol–gel technique. *J. Adv. Dielectr.* **2018**, *8*, 1850030. [CrossRef]
54. Ansari, F.; Sobhani, A.; Salavati-Niasari, M. Simple sol-gel synthesis and characterization of new $CoTiO_3/CoFe_2O_4$ nanocomposite by using liquid glucose, maltose and starch as fuel, capping and reducing agents. *J. Colloid Interface Sci.* **2018**, *514*, 723–732. [CrossRef]
55. Raut, A.V.; Barkule, R.S.; Shengule, D.R.; Jadhav, K.M. Synthesis, structural investigation and magnetic properties of Zn^{2+} substituted cobalt ferrite nanoparticles prepared by the sol–gel auto-combustion technique. *J. Magn. Magn. Mater.* **2014**, *358*, 87–92. [CrossRef]
56. Sajjia, M.; Oubaha, M.; Hasanuzzaman, M.; Olabi, A.G. Developments of cobalt ferrite nanoparticles prepared by the sol–gel process. *Ceram. Int.* **2014**, *40*, 1147–1154. [CrossRef]
57. Jain, S.R.; Adiga, K.C.; Verneker, V.P. A new approach to thermochemical calculations of condensed fuel-oxidizer mixtures. *Combust. Flame* **1981**, *40*, 71–79. [CrossRef]
58. Mapossa, A.B.; Dantas, J.; Costa, A.C. Transesterification reaction for biodiesel production from soybean oil using $Ni_{0.5}Zn_{0.5}Fe_2O_4$ nanomagnetic catalyst: Kinetic study. *Int. J. Energy Res.* **2020**, *44*, 6674–6684. [CrossRef]
59. Dantas, J.; Leal, E.; Mapossa, A.B.; Pontes, J.R.; Freitas, N.L.; Fernandes, P.C.; Costa, A.C.F. Biodiesel production on bench scale from different sources of waste oils by using NiZn magnetic heterogeneous nanocatalyst. *Int. J. Energy Res.* **2021**, *45*, 10924–10945. [CrossRef]
60. Costa, A.C.F.M.; Morelli, M.R.; Kiminami, R.H.G.A. Combustion synthesis: Effect of urea on the reaction and characteristics of Ni-Zn ferrite powders. *J. Mater. Synth. Process.* **2002**, *9*, 347–352. [CrossRef]
61. Hwang, C.C.; Tsai, J.S.; Huang, T.H.; Peng, C.H.; Chen, S.Y. Combustion synthesis of Ni–Zn ferrite powder—influence of oxygen balance value. *J. Solid State Chem.* **2005**, *178*, 382–389. [CrossRef]
62. Kombaiah, K.; Vijaya, J.J.; Kennedy, L.J.; Bououdina, M.; Al-Lohedan, H.A.; Ramalingam, R.J. Studies on Opuntia dilenii haw mediated multifunctional $ZnFe_2O_4$ nanoparticles: Optical, magnetic and catalytic applications. *Mater. Chem. Phys.* **2017**, *194*, 153–164. [CrossRef]
63. Segadães, A.M.; Morelli, M.R.; Kiminami, R.H.G.A. Combustion synthesis of aluminium titanate. *J. Eur. Ceram. Soc.* **1998**, *8*, 771–781. [CrossRef]
64. Mapossa, A.B.; Dantas, J.; Kiminami, A.G.H.R.; Silva, M.R.; Costa, A.C.F.M. Síntese do ferroespinélio $ZnFe_2O_4$ e avaliação do seu desempenho em reações de esterificação e transesterificação via rota metílica. *Rev. Eletrônica Mater. Process.* **2015**, *10*, 137–143.
65. Salunkhe, A.B.; Khot, V.M.; Phadatare, M.R.; Pawar, S.H. Combustion synthesis of cobalt ferrite nanoparticles—Influence of fuel to oxidizer ratio. *J. Alloys Compd.* **2012**, *514*, 91–96. [CrossRef]
66. Khorrami, S.A.; Manuchehri, Q.S. Magnetic properties of cobalt ferrite synthesized by hydrothermal and co-precipitation methods: A comparative study. *J. Appl. Chem. Res.* **2013**, *7*, 15–23.
67. Ren, Y.; Lin, L.; Ma, J.; Yang, J.; Feng, J.; Fan, Z. Sulfate radicals induced from peroxymonosulfate by magnetic ferrospinel MFe_2O_4 (M = Co, Cu, Mn, and Zn) as heterogeneous catalysts in the water. *Appl. Catal. B Environ.* **2015**, *165*, 572–578. [CrossRef]
68. Soto-Arreola, A.; Huerta-Flores, A.M.; Mora-Hernández, J.M.; Torres-Martínez, L.M. Comparative study of the photocatalytic activity for hydrogen evolution of MFe_2O_4 (M = Cu, Ni) prepared by three different methods. *J. Photochem. Photobiol. A Chem.* **2018**, *357*, 20–29. [CrossRef]
69. Rameshbabu, R.; Kumar, N.; Karthigeyan, A.; Neppolian, B. Visible light photocatalytic activities of $ZnFe_2O_4/ZnO$ nanoparticles for the degradation of organic pollutants. *Mater. Chem. Phys.* **2016**, *181*, 106–115. [CrossRef]
70. Jacinto, M.J.; Ferreira, L.F.; Silva, V.C. Magnetic materials for photocatalytic applications—A review. *J. Sol-Gel Sci. Technol.* **2020**, *96*, 1–14. [CrossRef]
71. Hassan, N.S.; Jalil, A.A. A review on self-modification of zirconium dioxide nanocatalysts with enhanced visible-light-driven photodegradation of organic pollutants. *J. Hazard. Mater.* **2022**, *423*, 126996. [CrossRef]
72. Suresh, R.; Rajendran, S.; Kumar, P.S.; Vo, D.V.N.; Cornejo-Ponce, L. Recent advancements of spinel ferrite based binary nanocomposite photocatalysts in wastewater treatment. *Chemosphere* **2021**, *274*, 129734. [CrossRef]
73. Li, F.; Liu, J.; Evans, D.G.; Duan, X. Stoichiometric synthesis of pure MFe_2O_4 (M = Mg, Co, and Ni) spinel ferrites from tailored layered double hydroxide (hydrotalcite-like) precursors. *Chem. Mater.* **2004**, *16*, 1597–1602. [CrossRef]
74. Tiwari, R.; De, M.; Tewari, H.S.; Ghoshal, S.K. Structural and magnetic properties of tailored $NiFe_2O_4$ nanostructures synthesized using auto-combustion method. *Results Phys.* **2020**, *16*, 102916. [CrossRef]
75. Vepulanont, K.; Sa-Nguanprang, S.; Buapoon, S.; Bunluesak, T.; Suebsom, P.; Chaisong, K.; Udomsri, N.; Karnchana, N.; Laokae, D.; Chanadee, T. Nickel ferrite ceramics: Combustion synthesis, sintering, characterization, and magnetic and electrical properties. *J. Asian Ceram. Soc.* **2021**, *9*, 639–651. [CrossRef]
76. Adeleke, J.T.; Theivasanthi, T.; Thiruppathi, M.; Swaminathan, M.; Akomolafe, T.; Alabi, A.B. Photocatalytic degradation of methylene blue by $ZnO/NiFe_2O_4$ nanoparticles. *Appl. Surf. Sci.* **2018**, *455*, 195–200. [CrossRef]
77. Hou, X.; Feng, J.; Liu, X.; Ren, Y.; Fan, Z.; Wei, T.; Meng, J.; Zhang, M. Synthesis of 3D porous ferromagnetic $NiFe_2O_4$ and using as novel adsorbent to treat wastewater. *J. Colloid Interface Sci.* **2011**, *362*, 477–485. [CrossRef]

78. Verma, K.C.; Singh, V.P.; Ram, M.; Shah, J.; Kotnala, R.K. Structural, microstructural and magnetic properties of $NiFe_2O_4$, $CoFe_2O_4$ and $MnFe_2O_4$ nanoferrite thin films. *J. Magn. Magn. Mater.* **2011**, *323*, 3271–3275. [CrossRef]
79. Xiong, P.; Fu, Y.; Wang, L.; Wang, X. Multi-walled carbon nanotubes supported nickel ferrite: A magnetically recyclable photocatalyst with high photocatalytic activity on degradation of phenols. *Chem. Eng. J.* **2012**, *195*, 149–157. [CrossRef]
80. Peng, T.; Zhang, X.; Lv, H.; Zan, L. Preparation of $NiFe_2O_4$ nanoparticles and its visible-light-driven photoactivity for hydrogen production. *Catal. Commun.* **2012**, *28*, 116–119. [CrossRef]
81. Ren, A.; Liu, C.; Hong, Y.; Shi, W.; Lin, S.; Li, P. Enhanced visible-light-driven photocatalytic activity for antibiotic degradation using magnetic $NiFe_2O_4/Bi_2O_3$ heterostructures. *Chem. Eng. J.* **2014**, *258*, 301–308. [CrossRef]
82. Bhosale, S.V.; Kanhe, N.S.; Bhoraskar, S.V.; Bhat, S.K.; Bulakhe, R.N.; Shim, J.J.; Mathe, V.L. Micro-structural analysis of $NiFe_2O_4$ nanoparticles synthesized by thermal plasma route and its suitability for BSA adsorption. *J. Mater. Sci. Mater. Med.* **2015**, *26*, 1–15. [CrossRef] [PubMed]
83. Khosravi, I.; Eftekhar, M. Characterization and evaluation catalytic efficiency of $NiFe_2O_4$ nano spinel in removal of reactive dye from aqueous solution. *Powder Technol.* **2013**, *250*, 147–153. [CrossRef]
84. Hung, D.Q.; Thanh, N.K. Preparation of $NiFe_2O_4$-TiO_2 nanoparticles and study of their photocatalytic activity. *VNU J. Sci. Math.-Phys.* **2011**, *27*, 204–211.
85. Shao, R.; Sun, L.; Tang, L.; Chen, Z. Preparation and characterization of magnetic core–shell $ZnFe_2O_4$@ZnO nanoparticles and their application for the photodegradation of methylene blue. *Chem. Eng. J.* **2013**, *217*, 185–191. [CrossRef]
86. Fan, G.; Gu, Z.; Yang, L.; Li, F. Nanocrystalline zinc ferrite photocatalysts formed using the colloid mill and hydrothermal technique. *Chem. Eng. J.* **2009**, *155*, 534–541. [CrossRef]
87. Cheng, P.; Li, W.; Zhou, T.; Jin, Y.; Gu, M. Physical and photocatalytic properties of zinc ferrite doped titania under visible light irradiationJ. *Photochem. Photobiol. A Chem.* **2004**, *168*, 97–101. [CrossRef]
88. Su, M.; He, C.; Sharma, V.K.; Abou Asi, M.; Xia, D.; Li, X.Z.; Deng, H.; Xiong, Y. Mesoporous zinc ferrite: Synthesis, characterization, and photocatalytic activity with H_2O_2/visible light. *J. Hazard. Mater.* **2012**, *211*, 95–103. [CrossRef]
89. Mahmoodi, N.M. Zinc ferrite nanoparticle as a magnetic catalyst: Synthesis and dye degradation. *Mater. Res. Bull.* **2013**, *48*, 4255–4260. [CrossRef]
90. Guo, X.; Zhu, H.; Li, Q. Visible-light-driven photocatalytic properties of ZnO/$ZnFe_2O_4$ core/shell nanocable arrays. *Appl. Catal. B Environ.* **2014**, *160*, 408–414. [CrossRef]
91. Yuan, Z.H. Synthesis, characterization and photocatalyticactivity of $ZnFe_2O_4/TiO_2$ nanocomposite. *J. Mater. Chem.* **2001**, *11*, 1265–1268. [CrossRef]
92. Hou, X.; Feng, J.; Xu, X.; Zhang, M. Synthesis and characterizations of spinel $MnFe_2O_4$ nanorod by seed–hydrothermal route. *J. Alloys Compd.* **2010**, *491*, 258–263. [CrossRef]
93. Patil, S.B.; Naik, H.B.; Nagaraju, G.; Viswanath, R.; Rashmi, S.K. Sugarcane juice mediated eco-friendly synthesis of visible light active zinc ferrite nanoparticles: Application to degradation of mixed dyes and antibacterial activities. *Mater. Chem. Phys.* **2018**, *212*, 351–362. [CrossRef]
94. Sripriya, R.C.; Vigneaswari, B.; Raj, V.A. Comparative Studies of Magneto-Optical and Photocatalytic Properties of Magnetically Recyclable Spinel $ZnFe_2O_4$ Nanostructures by Combustion Methods. *Int. J. Nanosci.* **2019**, *18*, 1850020. [CrossRef]
95. Dutta, V.; Sharma, S.; Raizada, P.; Hosseini-Bandegharaei, A.; Gupta, V.K.; Singh, P. Review on augmentation in photocatalytic activity of $CoFe_2O_4$ via heterojunction formation for photocatalysis of organic pollutants in water. *J. Saudi Chem. Soc.* **2019**, *23*, 1119–1136.
96. Sickafus, K.E.; Wills, J.M.; Grimes, N.W. Structure of spinel. *J. Am. Ceram. Soc.* **1999**, *82*, 3279–3292. [CrossRef]
97. Zheng, J.; Song, X.; Liu, X.; Chen, W.; Li, Y.; Guo, J. Synthesis of hexagonal $CoFe_2O_4$/ZnO nanoparticles and their electromagnetic properties. *Mater. Lett.* **2012**, *73*, 143–146. [CrossRef]
98. Sathishkumar, P.; Mangalaraja, R.V.; Anandan, S.; Ashokkumar, M. $CoFe_2O_4/TiO_2$ nanocatalysts for the photocatalytic degradation of Reactive Red 120 in aqueous solutions in the presence and absence of electron acceptors. *Chem. Eng. J.* **2013**, *220*, 302–310. [CrossRef]
99. Moosavi, S.M.; Molla-Abbasi, P.; Haji-Aghajani, Z. Photo-catalyst $CoFe_2O_4$–TiO_2: Application in photo-degradation of organic dyes and magnetic nanocomposite preparation. *J. Mater. Sci. Mater. Electron.* **2016**, *27*, 4879–4886. [CrossRef]
100. Krishna, S.; Sathishkumar, P.; Pugazhenthiran, N.; Guesh, K.; Mangalaraja, R.V.; Kumaran, S.; Gracia-Pinilla, M.A.; Anandan, S. Heterogeneous sonocatalytic activation of peroxomonosulphate in the presence of $CoFe_2O_4/TiO_2$ nanocatalysts for the degradation of Acid Blue 113 in an aqueous environment. *J. Environ. Chem. Eng.* **2020**, *8*, 104024.
101. Li, C.J.; Wang, J.N.; Wang, B.; Gong, J.R.; Lin, Z. A novel magnetically separable $TiO_2/CoFe_2O_4$ nanofiber with high photocatalytic activity under UV–vis light. *Mater. Res. Bull.* **2012**, *47*, 333–337. [CrossRef]
102. Chandel, N.; Sharma, K.; Sudhaik, A.; Raizada, P.; Hosseini-Bandegharaei, A.; Thakur, V.K.; Singh, P. Magnetically separable ZnO/$ZnFe_2O_4$ and ZnO/$CoFe_2O_4$ photocatalysts supported onto nitrogen doped graphene for photocatalytic degradation of toxic dyes. *Arab. J. Chem.* **2020**, *13*, 4324–4340. [CrossRef]
103. Arief, S.; Jamarun, N.; Stiadi, Y. Magnetically separable ZnO-$MnFe_2O_4$ nanocomposites synthesized in organic-free media for dye degradation under natural sunlight. *Orient. J. Chem.* **2017**, *33*, 2758.
104. Akhlaghi, N.; Najafpour-Darzi, G. Manganese ferrite ($MnFe_2O_4$) Nanoparticles: From synthesis to application—A review. *J. Ind. Eng. Chem.* **2021**, *103*, 292–304. [CrossRef]

105. Deraz, N.M.; Shaban, S. Optimization of catalytic, surface and magnetic properties of nanocrystalline manganese ferrite. *J. Anal. Appl. Pyrol.* **2009**, *86*, 173–179. [CrossRef]
106. Chang, L.; Pu, Y.; Jing, P.; Cui, Y.; Zhang, G.; Xu, S.; Cao, B.; Guo, J.; Chen, F.; Qiao, C. Magnetic core-shell $MnFe_2O_4$@TiO_2 nanoparticles decorated on reduced graphene oxide as a novel adsorbent for the removal of ciprofloxacin and Cu(II) from water. *Appl. Surf. Sci.* **2021**, *541*, 148400. [CrossRef]
107. Zamani, A.; Seyed Sadjadi, M.; Mahjoub, A.R.; Yousefi, M.; Farhadyar, N. Synthesis and characterization $ZnFe_2O_4$@MnO and $MnFe_2O_4$@ZnO magnetic nanocomposites: Investigation of photocatalytic activity for the degradation of Congo Red under visible light irradiation. *Int. J. Nano Dimens.* **2020**, *11*, 58–73.
108. Silambarasu, A.; Manikandan, A.; Balakrishnan, K.; Jaganathan, S.K.; Manikandan, E.; Aanand, J.S. Comparative study of structural, morphological, magneto-optical and photo-catalytic properties of magnetically reusable spinel $MnFe_2O_4$ nano-catalysts. *J. Nanosci. Nanotechnol.* **2018**, *18*, 3523–3531. [CrossRef] [PubMed]
109. Golshan, M.; Kakavandi, B.; Ahmadi, M.; Azizi, M. Photocatalytic activation of peroxymonosulfate by TiO_2 anchored on cupper ferrite (TiO_2@$CuFe_2O_4$) into 2,4-D degradation: Process feasibility, mechanism and pathway. *J. Hazard. Mater.* **2018**, *359*, 325–337. [CrossRef] [PubMed]
110. Anandan, S.; Selvamani, T.; Prasad, G.G.; Asiri, A.M.; Wu, J.J. Magnetic and catalytic properties of inverse spinel $CuFe_2O_4$ nanoparticles. *J. Magn. Magn. Mater.* **2017**, *432*, 437–443. [CrossRef]
111. You-Yi, Y.; Heng-Qiang, Z. Reduced graphene oxide coupled magnetic $CuFe_2O_4$-TiO_2 nanoparticles with enhanced photocatalytic activity for methylene blue degradation. *Struct Chem.* **2016**, *35*, 472–480.
112. Shevale, V.B.; Dhodamani, A.G.; Delekar, S.D. Catalytic reclamation of silver present in photographic waste using magnetically separable TiO_2@$CuFe_2O_4$ nanocomposites and thereof its use in antibacterial activity. *ACS Omega* **2020**, *5*, 1098–1108. [CrossRef]
113. Janani, B.; Syed, A.; Thomas, A.M.; Al-Rashed, S.; Elgorban, A.M.; Raju, L.L.; Khan, S.S. A simple approach for the synthesis of bi-functional pn type ZnO@$CuFe_2O_4$ heterojunction nanocomposite for photocatalytic and antimicrobial application. *Phys. E Low-Dimens. Syst. Nanostruct.* **2021**, *130*, 114664. [CrossRef]
114. Zhang, C.F.; Zhong, X.C.; Yu, H.Y.; Liu, Z.W.; Zeng, D.C. Effects of cobalt doping on the microstructure and magnetic properties of Mn–Zn ferrites prepared by the co-precipitation method. *Phys. B Condens. Matter.* **2009**, *404*, 2327–2331. [CrossRef]
115. Manikandan, A.; Durka, M.; Antony, S.A. Magnetically recyclable spinel $Mn_xZn_{1-x}Fe_2O_4$ ($0.0 \leq x \leq 0.5$) nano-photocatalysts. *Adv. Sci. Eng. Med.* **2015**, *7*, 33–46. [CrossRef]
116. Shaikh, P.A.; Kambale, R.C.; Rao, A.V.; Kolekar, Y.D. Structural, magnetic and electrical properties of Co–Ni–Mn ferrites synthesized by co-precipitation method. *J. Alloys Compd.* **2010**, *492*, 590–596. [CrossRef]
117. Ciocarlan, R.G.; Seftel, E.M.; Mertens, M.; Pui, A.; Mazaj, M.; Tusar, N.N.; Cool, P. Novel magnetic nanocomposites containing quaternary ferrites systems $Co_{0.5}Zn_{0.25}M_{0.25}Fe_2O_4$ (M = Ni, Cu, Mn, Mg) and TiO_2-anatase phase as photocatalysts for wastewater remediation under solar light irradiation. *Mater. Sci. Eng. B* **2018**, *230*, 1–7. [CrossRef]
118. Jesudoss, S.K.; Vijaya, J.J.; Kennedy, L.J.; Rajan, P.I.; Al-Lohedan, H.A.; Ramalingam, R.J.; Kaviyarasu, K.; Bououdina, M. Studies on the efficient dual performance of $Mn_{1-x}Ni_xFe_2O_4$ spinel nanoparticles in photodegradation and antibacterial activity. *J. Photochem. Photobiol. B Biol.* **2016**, *165*, 121–132. [CrossRef]
119. Naik, M.M.; Naik, H.B.; Nagaraju, G.; Vinuth, M.; Vinu, K.; Viswanath, R. Green synthesis of zinc doped cobalt ferrite nanoparticles: Structural, optical, photocatalytic and antibacterial studies. *Nano-Struct. Nano-Objects.* **2019**, *19*, 100322. [CrossRef]
120. Baig, M.M.; Pervaiz, E.; Afzal, M.J. Catalytic activity and kinetic studies of Core@ Shell nanostructure $NiFe_2O_4$@TiO_2 for photocatalytic degradation of methyl orange dye. *J. Chem. Soc. Pak.* **2020**, *42*, 531.
121. Baldrian, P.; Merhautová, V.; Gabriel, J.; Nerud, F.; Stopka, P.; Hrubý, M.; Beneš, M.J. Decolorization of synthetic dyes by hydrogen peroxide with heterogeneous catalysis by mixed iron oxides. *Appl. Catal. B Environ.* **2006**, *66*, 258–264. [CrossRef]
122. Neris, A.M.; Schreiner, W.H.; Salvador, C.; Silva, U.C.; Chesman, C.; Longo, E.; Santos, I.M.G. Photocatalytic evaluation of the magnetic core@ shell system (Co, Mn) Fe_2O_4@TiO_2 obtained by the modified Pechini method. *Mater. Sci. Eng. B* **2018**, *229*, 218–226. [CrossRef]
123. Cao, X.; Gu, L.; Lan, X.; Zhao, C.; Yao, D.; Sheng, W. Spinel $ZnFe_2O_4$ nanoplates embedded with Ag clusters: Preparation, characterization, and photocatalytic application. *Mater. Chem. Phys.* **2007**, *106*, 175–180. [CrossRef]
124. Zhang, G.Y.; Sun, Y.Q.; Gao, D.Z.; Xu, Y.Y. Quasi-cube $ZnFe_2O_4$ nanocrystals: Hydrothermal synthesis and photocatalytic activity with TiO_2 (Degussa P25) as nanocomposite. *Mater. Res. Bull.* **2010**, *45*, 755–760. [CrossRef]
125. Zhang, B.; Zhang, J.; Chen, F. Preparation and characterization of magnetic TiO_2/$ZnFe_2O_4$ photocatalysts by a sol–gel method. *Res. Chem. Intermed.* **2008**, *34*, 375–380. [CrossRef]
126. Li, X.; Hou, Y.; Zhao, Q.; Wang, L. A general, one-step and template-free synthesis of sphere-like zinc ferrite nanostructures with enhanced photocatalytic activity for dye degradation. *J. Colloid Interface Sci.* **2011**, *358*, 102–108. [CrossRef]
127. Li, H.; Zhang, Y.; Wang, S.; Wu, Q.; Liu, C. Study on nanomagnets supported TiO_2 photocatalysts prepared by a sol–gel process in reverse microemulsion combining with solvent-thermal technique. *J. Hazard. Mater.* **2009**, *169*, 1045–1053. [CrossRef]
128. Fu, Y.P.; Chang, W.K.; Wang, H.C.; Liu, C.W.; Lin, C.H. Synthesis and characterization of anatase TiO_2 nanolayer coating on Ni–Cu–Zn ferrite powders for magnetic photocatalyst. *J. Mater. Res.* **2010**, *25*, 134–140. [CrossRef]
129. Dom, R.; Subasri, R.; Radha, K.; Borse, P.H. Synthesis of solar active nanocrystalline ferrite, MFe_2O_4 (M: Ca, Zn, Mg) photocatalyst by microwave irradiation. *Solid State Commun.* **2011**, *151*, 470–473. [CrossRef]

130. Chen, C.H.; Liang, Y.H.; Zhang, W.D. $ZnFe_2O_4$/MWCNTs composite with enhanced photocatalytic activity under visible-light irradiation. *J. Alloys Compd.* **2010**, *501*, 168–172. [CrossRef]
131. Rana, S.; Srivastava, R.S.; Sorensson, M.M.; Misra, R.D.K. Synthesis and characterization of nanoparticles with magnetic core and photocatalytic shell: Anatase TiO_2–$NiFe_2O_4$ system. *Mater. Sci. Eng. B* **2005**, *119*, 144–151. [CrossRef]
132. Cheng, P.; Deng, C.; Gu, M.; Shangguan, W. Visible-light responsive zinc ferrite doped titania photocatalyst for methyl orange degradation. *J. Mater. Sci.* **2007**, *42*, 9239–9244. [CrossRef]
133. Jadhav, S.D.; Hankare, P.P.; Patil, R.P.; Sasikala, R. Effect of sintering on photocatalytic degradation of methyl orange using zinc ferrite. *Mater. Lett.* **2011**, *65*, 371–373. [CrossRef]
134. Xu, S.; Feng, D.; Shangguan, W. Preparations and photocatalytic properties of visible-light-active zinc ferrite-doped TiO_2 photocatalyst. *J. Phys. Chem. C* **2009**, *113*, 2463–2467. [CrossRef]
135. Arifin, M.N.; Karim, K.M.R.; Abdullah, H.; Khan, M.R. Synthesis of titania doped copper ferrite photocatalyst and its photoactivity towards methylene blue degradation under visible light irradiation. *Bull. Chem. React. Eng. Catal.* **2019**, *14*, 219–227. [CrossRef]
136. Zouhier, M.; Tanji, K.; Navio, J.A.; Hidalgo, M.C.; Jaramillo-Páez, C.; Kherbeche, A. Preparation of $ZnFe_2O_4$/ZnO composite: Effect of operational parameters for photocatalytic degradation of dyes under UV and visible illumination. *J. Photochem. Photobiol. A Chem.* **2020**, *390*, 112305. [CrossRef]
137. To Loan, N.T.; Hien Lan, N.T.; Thuy Hang, N.T.; Quang Hai, N.; Tu Anh, D.T.; Thi Hau, V.; Van Tan, L.; Van Tran, T. $CoFe_2O_4$ nanomaterials: Effect of annealing temperature on characterization, magnetic, photocatalytic, and photo-fenton properties. *Processes* **2019**, *7*, 885. [CrossRef]
138. Mir, S.H.; Jennings, B.D.; Akinoglu, G.E.; Selkirk, A.; Gatensby, R.; Mokarian-Tabari, P. Enhanced Dye Degradation through Multi-Particle Confinement in a Porous Silicon Substrate: A Highly Efficient, Low Band Gap Photocatalyst. *Adv. Opt. Mater.* **2021**, *9*, 2002238. [CrossRef]
139. Sciortino, F.; Sanchez-Ballester, N.M.; Mir, S.H.; Rydzek, G. Functional Elastomeric Copolymer Membranes Designed by Nanoarchitectonics Approach for Methylene Blue Removal. *J. Inorg. Organomet. Polym.* **2021**, *31*, 1967–1977. [CrossRef]
140. Velmurugan, R.; Swaminathan, M. An efficient nanostructured ZnO for dye sensitized degradation of Reactive Red 120 dye under solar light. *Sol. Energy Mater Sol. Cells.* **2011**, *95*, 942–950. [CrossRef]
141. Selvam, K.; Balachandran, S.; Velmurugan, R.; Swaminathan, M. Mesoporous nitrogen doped nano titania—A green photocatalyst for the effective reductive cleavage of azoxybenzenes to amines or 2-phenyl indazoles in methanol. *Appl. Catal. A Gen.* **2012**, *413*, 213–222. [CrossRef]
142. Mathubala, G.; Manikandan, A.; Antony, S.A.; Ramar, P. Photocatalytic degradation of methylene blue dye and magneto-optical studies of magnetically recyclable spinel $Ni_xMn_{1-x}Fe_2O_4$ (x = 0.0–1.0) nanoparticles. *J. Mol. Struct.* **2016**, *1113*, 79–87. [CrossRef]
143. Leonel, A.G.; Mansur, A.A.; Mansur, H.S. Advanced Functional Nanostructures based on Magnetic Iron Oxide Nanomaterials for Water Remediation: A Review. *Water Res.* **2020**, *190*, 116693. [CrossRef]
144. Padmapriya, G.; Manikandan, A.; Krishnasamy, V.; Jaganathan, S.K.; Antony, S.A. Spinel $Ni_xZn_{1-x}Fe_2O_4$ ($0.0 \leq x \leq 1.0$) nano-photocatalysts: Synthesis, characterization and photocatalytic degradation of methylene blue dye. *J. Mol. Struct.* **2016**, *1119*, 39–47. [CrossRef]
145. Jia, Z.; Ren, D.; Liang, Y.; Zhu, R. A new strategy for the preparation of porous zinc ferrite nanorods with subsequently light-driven photocatalytic activity. *Mater. Lett.* **2011**, *65*, 3116–3119. [CrossRef]
146. Velmurugan, R.; Krishnakumar, B.; Subash, B.; Swaminathan, M. Preparation and characterization of carbon nanoparticles loaded TiO_2 and its catalytic activity driven by natural sunlight. *Sol. Energy Mater Sol. Cells* **2013**, *108*, 205–212. [CrossRef]
147. Mandal, S.S.; Bhattacharyya, A.J. Electrochemical sensing and photocatalysis using Ag–TiO_2 microwires. *J. Chem. Sci.* **2012**, *124*, 969–978. [CrossRef]
148. Kumar, A.; Pandey, G. A review on the factors affecting the photocatalytic degradation of hazardous materials. *Mater. Sci. Eng. Int. J.* **2017**, *1*, 1–10. [CrossRef]
149. Mirkhani, V.; Tangestaninejad, S.; Moghadam, M.; Habibi, M.H.; Rostami-Vartooni, A. Photocatalytic degradation of azo dyes catalyzed by Ag doped TiO_2 photocatalyst. *J. Iran. Chem. Soc.* **2009**, *6*, 578–587. [CrossRef]
150. Suwarnkar, M.B.; Dhabbe, R.S.; Kadam, A.N.; Garadkar, K.M. Enhanced photocatalytic activity of Ag doped TiO_2 nanoparticles synthesized by a microwave assisted method. *Ceram. Int.* **2014**, *40*, 5489–5496. [CrossRef]
151. Zhu, X.; Zhang, F.; Wang, M.; Ding, J.; Sun, S.; Bao, J.; Gao, C. Facile synthesis, structure and visible light photocatalytic activity of recyclable $ZnFe_2O_4$/TiO_2. *Appl. Surf. Sci.* **2014**, *319*, 83–89. [CrossRef]
152. Gupta, V.K.; Eren, T.; Atar, N.; Yola, M.L.; Parlak, C.; Karimi-Maleh, H. $CoFe_2O_4$@TiO_2 decorated reduced graphene oxide nanocomposite for photocatalytic degradation of chlorpyrifos. *J. Mol. Liq.* **2015**, *208*, 122–129. [CrossRef]
153. Haw, C.; Chiu, W.; Rahman, S.A.; Khiew, P.; Radiman, S.; Shukor, R.A.; Hamid, M.A.A.; Ghazali, N. The design of new magnetic-photocatalyst nanocomposites ($CoFe_2O_4$–TiO_2) as smart nanomaterials for recyclable-photocatalysis applications. *New J. Chem.* **2016**, *40*, 1124–1136. [CrossRef]
154. Ahmadpour, N.; Sayadi, M.H.; Sobhani, S.; Hajiani, M. A potential natural solar light active photocatalyst using magnetic $ZnFe_2O_4$@TiO_2/Cu nanocomposite as a high performance and recyclable platform for degradation of naproxen from aqueous solution. *J. Clean. Prod.* **2020**, *268*, 122023. [CrossRef]
155. Nguyen, T.B.; Doong, R.A. Fabrication of highly visible-light-responsive $ZnFe_2O_4$/TiO_2 heterostructures for the enhanced photocatalytic degradation of organic dyes. *RSC Adv.* **2016**, *6*, 103428–103437. [CrossRef]

156. Xu, S.H.; Feng, D.L.; Li, D.X.; Shangguan, W.F. Preparation of magnetic photocatalyst TiO_2 supported on $NiFe_2O_4$ and effect of magnetic carrier on photocatalytic activity. *Chin. J. Chem.* **2008**, *26*, 842–846. [CrossRef]
157. Nguyen, T.B.; Huang, C.P.; Doong, R.A. Photocatalytic degradation of bisphenol A over a $ZnFe_2O_4/TiO_2$ nanocomposite under visible light. *Sci. Total Environ.* **2019**, *646*, 745–756. [CrossRef]
158. Saad, D.; Byrne, D.; Drechsel, P. Social perspectives on the effective management of wastewater. In *Physico-Chemical Wastewater Treatment and Resource Recovery*; Farooq, R., Ahmad, Z., Eds.; InTech: London, UK, 2017; pp. 253–267.
159. Wichelns, D.; Drechsel, P.; Qadir, M. Wastewater: Economic Asset in an Urbanizing World. In *Wastewater*; Drechsel, P., Qadir, M., Wichelns, D., Eds.; Springer: Dordrecht, The Netherlands, 2015; pp. 3–14.
160. Friedler, E.; Lahav, O.; Jizhaki, H.; Lahav, T. Study of urban population attitudes towards various wastewater reuse options: Israel as a case study. *J. Environ. Manag.* **2006**, *81*, 360–370. [CrossRef]
161. Gebrezgabher, S.; Rao, K.; Hanjra, M.A.; Hernández-Sancho, F. Business models and economic approaches for recovering energy from wastewater and fecal sludge. In *Wastewater*; Springer: Dordrecht, The Netherlands, 2015; pp. 217–245.